TECHNISCHE
UNIVERSITÄT
WIEN
Vienna University of Technology

D I P L O M A R B E I T

Investigation of the prompt gamma ray emission for on-line monitoring in ion therapy

ausgeführt am

Atominstitut
der Technischen Universität Wien

und an der
Österreichischen Akademie der Wissenschaften

unter der Anleitung von
Privatdoz. Dipl. Ing. Dr. Johann Marton

durch

Dominik Steinschaden

Frauenberggasse 1d
3552 Lengenfeld

———————————   ———————————
Datum   Unterschrift

Note of thanks

I want to thank my supervisor at the Stefan-Meyer Institute Dr. Johann Marton who made this work possible. Furthermore I want to thank Dr. Albert Hirtl and Dipl.-Ing. Hermann Fuchs from the AKH Vienna who supported me with the necessary medical and physical knowledge as well as the access to the computer cluster of the AKH Vienna and the used software toolkit. Finally I want to thank my colleagues Harald Dichtl and Andreas Pichler who worked with me on the project and provided me a lot.

Kurzfassung

Diese Diplomarbeit beschaeftigt sich mit der Untersuchung der Emission und dem Verhalten von prompten Gamma-Photonen bei der Ionentherapie mit Kohlenstoffionen. Das Ziel dieser Untersuchung war die Entwicklung einer Methode, welche die durch Kernreaktionen des einfallenden Therapiestrahls mit dem bestrahlten Gewebe entstehenden prompten Gammastrahlen zur Bestimmung des Bragg-Peaks direkt waehrend der medizinischen Behandlung nutzt. Im Zuge dieser Arbeit wurden Monte Carlo Simulationen mit der Simulationsumgebung GATE (GEANT 4 Application for Tomographic Emission) am Rechencluster des Allgemeinen Krankenhauses (AKH) Wien durchgefuehrt. Dabei wurden verschiedene Entstehungsparameter der prompten Gamma-Photonen wie Produktionsrate, -richtung und -energie abhaengig von der Primaerenergie der Kohlenstoffionen und der Eindringtiefe in einem Wasservolumen untersucht und auf einen moeglichen Zusammenhang mit der Position des Bragg-Peaks und somit mit der Verteilung der abgegebenen Dosis ueberprueft. Dadurch konnte ein Energiebereich fuer die entstehenden Gammastrahlen ermittelt werden, in welchem die Produktionsrate der Photonen einen signifikanten Abfall unmittelbar nach dem Bragg-Peak aufweist. Außerdem wurde untersucht, ob die Photonen derartige Eigenschaften bis zum Austritt aus dem bestrahlten Medium behalten und sich dadurch fuer ein Monitoring eignen. Dafuer wurden das Streuverhalten von Photonen und deren Absorptionsraten bei entsprechenden Energien untersucht. Zusaetzlich wurde aus den untersuchten Entstehungsparametern und der Geometrie der virtuellen Anordnung eine Messung der prompten Gamma-Photonen außerhalb des bestrahlten Materials berechnet und das Ergebnis mit simulierten Messungen verglichen.

Abstract

This thesis deals with the investigation of the emission and the characteristics of prompt gamma rays in radiotherapy with carbon ions. The aim of this investigation was to develop a method which uses the prompt gamma rays, created by nuclear reactions of the incident therapy beam with the irradiated tissue, to determine the position of the Bragg peak during the medical treatment. The experiments of this work were carried out by Monte Carlo simulations in the framework of the simulation environment GATE (GEANT4 Application for Tomographic Emission) realized on the computer cluster of the Allgemeine Krankenhaus (AKH) Vienna. In the course of this investigations some production parameters of prompt gamma rays like the emission rate, energy and direction were measured as a function of the primary carbon ion energy and the penetration depth in a water target. A possible connection between these parameters and the position of the Bragg peak and the dose delivery was checked. An energy range for produced γ-rays can be detected in which the production rate of the photons shows a significant drop right after the Bragg peak. Furthermore the passage of the gamma rays outside the irradiated tissues prior to detection was examined in order to proof the availability for ion treatment monitoring. For that reason the scattering of photons and their absorption rate were investigated at the respective energies. Additional the measurement of prompt γ photons outside of the irradiated material was calculated with the help of the measured production parameters and the virtual geometry. Afterwards it was compared with the outcome of a simulated measurement outside the target.

Contents

1 Introduction

The treatment of cancer is with increasing frequency performed by radiotherapy with ions. Although there exist no satisfying method to monitor the influence of the iontherapy right during the treatment in the USA alone many thousands therapies are performed per year. Patients have to be examined by the use of existing imaging methods like computed tomography. The parameters for a radiotherapy like energy and duration get calculated but there is no system to proof if the right tissue is irradiated during the treatment. Only after the treatment with the help of PET monitoring the result of the therapy can be reviewed and the parameters adjusted for following treatments. Against this background the search for new methods to observe and thereby adapt a hadrontherapy with ions during the treatment is a vital topic. There are some attempts to use the prompt γ radiation, occurring during an iontherapy in the irradiated tissue for an online monitoring of the dose delivery and the beam path. This prompt radiation background, which is disturbing and preventing PET monitoring during treatment, is higher in regions of higher dose deposit and for that a detection of this γ photons may gives an opportunity to recalculate the beam path and the area of the Bragg peak [1].

The aim of this master thesis was to investigate the principle possibility of a prompt γ based monitoring. Based on Monte Carlo simulations the production parameters of the γ photons like energy spectra, site of production and direction of production during an irradiation of a human like target by a carbon ion beam were examined as well as the behaviour of this radiation while passing a human like volume. Build on this perceptions a method to detect the Bragg peak should be proposed.

2 Physical properties of ionizing radiation

Ionizing radiation describes these sorts of radiation which have the possibility to modify the atomic shells of the atoms of the matter, they are interacting with. For that reason these radiations ionize the irradiated material along their path. Concrete a positive ion occurs if an electron is displaced from a neutral atom. Because the electrons are bound in an atom the transferred energy to release them must be at least as high as the so called ionisation energy. For example the UV region is the transition area from non ionizing to ionizing radiation for photons. Not only electromagnetic radiation can be the cause of ionized atoms but also particle or hadron radiation like alpha or beta radiation. Since all of these radiations remove an electron from an atom or a molecule these radiations destroy the molecules or chemical compounds they are interacting with. For this reason they are used in different medical applications [2].

2.1 Interaction of ionizing photons with matter

Electromagnetic radiation can interact with matter by several different processes, whereby the probability for each process depends on the energy of the single photon and the properties of the material.

Photoelectric effect: If the photoelectric effect occurs the photon transfers its whole energy to an electron bound by an atom. One part of the energy is used to break the boundary and free the electron, while the rest is available as kinetic energy for the electron (cf. figure 2.1c on page 5).

Compton scattering: Also during the Compton effect a photon interacts with an electron of an atom, but instead of getting completely absorbed the photon is only scattered at a loosely bound electron. This electron again loses its bonds to the atom and takes some of the available energy as kinetic energy. Also the photon moves on, however with a changed frequency and direction to satisfy the momentum and energy conservation (cf. figure 2.1b).

Pair production: If the incoming photon has an energy even higher then double the rest energy of an electron, which means the energy is above 1.022 MeV, may a pair production occurs and the energy of the photon is used to produce an electron and a positron. Also for this process the photon must interact with an atom, because an atom core is needed to take up a part of the momentum of the photon to satisfy the momentum conservation. For the reason that the positron is the anti particle of the electron the range of the positron is quite low before it recombines with any electron of the matter and for this ionizes an atom and emits photons with an overall energy of 1.022 MeV(cf. figure 2.1d).

Elastic scattering: Additionally especially photons with low energies below 10 keV can get absorbed by an electron. This exited electron then can emit a photon of the same wavelength and frequency in an other direction. Because of the low energy this effect has nearly no relevance in radiotherapy and for the investigations in this master thesis(cf. figure 2.1).

If a photon beam passes through a certain area of a material the beam will be attenuated by the introduced processes. In formula 2.1 the attenuation is described by the use of the initial intensity P_0, the attenuation coefficient μ and the thickness x of the material.

$$P(x) = P_0 e^{-\mu x} \tag{2.1}$$

As apparent the attenuation happens in an exponential way and for this reason also the dose distribution in the material caused by the ionization shows an exponential decrease after a short build up phase. Figure 2.2 on page 6 shows a simulated dose distribution of a gamma beam in a water target [2].

2.2 Interaction of ionizing particles with matter

As distinct from photons particles like electrons, alpha particles or ions interact with matter predominately via Coulomb forces. Instead of an exponential decrease the dose profiles are characterized by the so called Bragg peak. Figure 2.3 on page 7 shows the dose profiles of ^{12}C ions with different energies and for comparison the dose profile of γ rays. The position of the Bragg peak can be adjusted exactly as a function of the primary energy of the ions and the properties of the irradiated material. Equation 2.2 describes the stopping of ions in an absorber.

$$\frac{dE}{dx} \approx \frac{Kn_0(Z_{eff})^2}{\beta^2} * [ln\frac{2m_e c^2 \beta^2}{I(1-\beta^2)} - \beta^2] \tag{2.2}$$
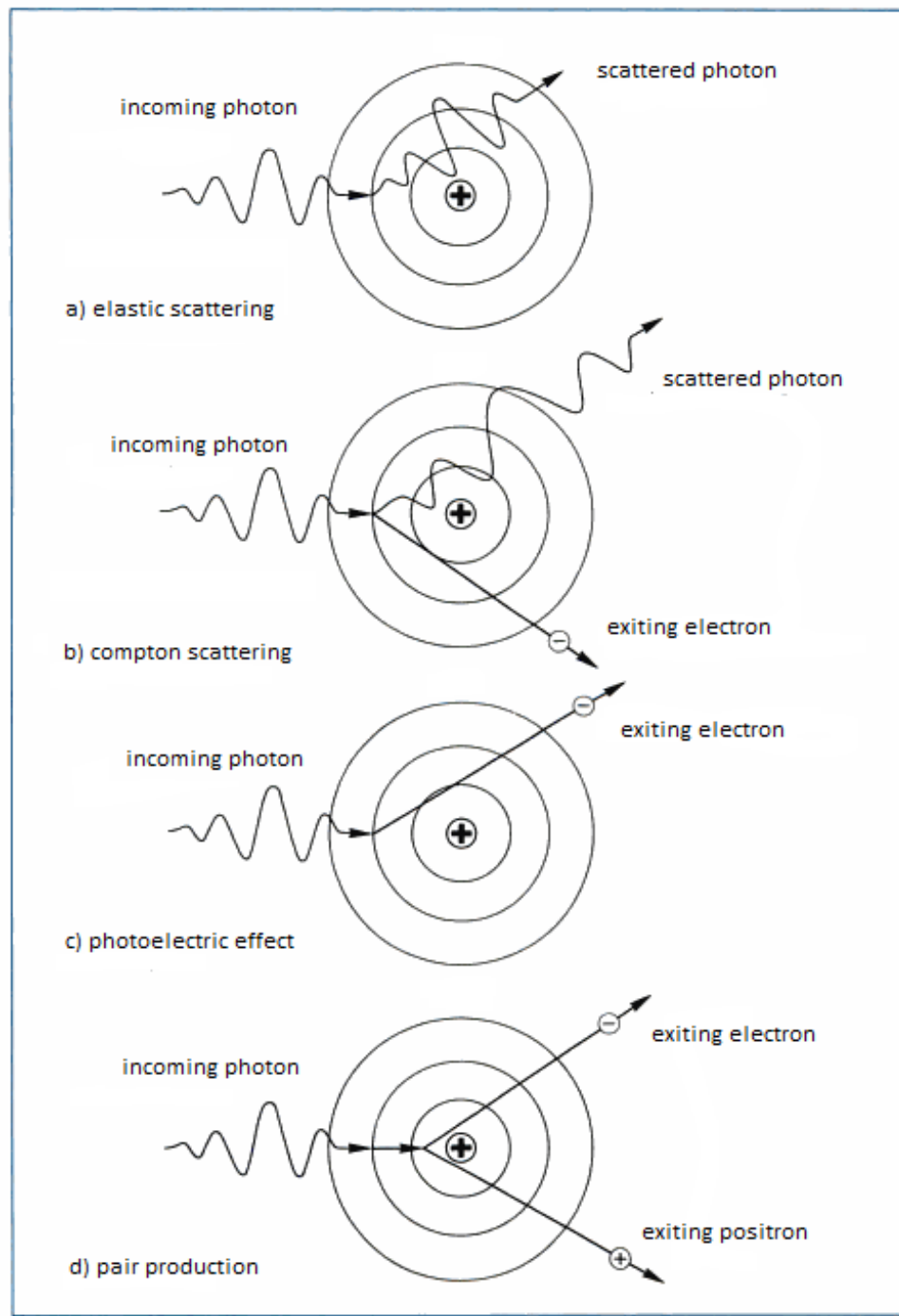
Figure 2.1: Interaction processes between ionizing photons and matter. a) elastic scattering, b) compton scattering, c) photoelectic effect, d) pair production [2]
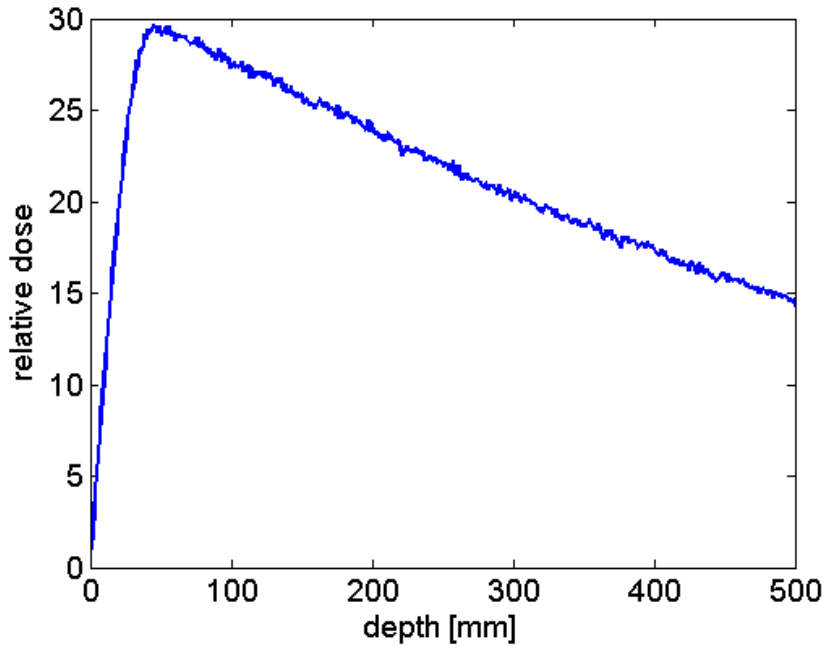
Figure 2.2: Simulated depth-dose distribution for 10 MeV photon radiation in water [3]

The energy loss $\frac{dE}{dx}$ depends on the electron density of the target material n_0, the effective charge of the projectile ions Z_{eff}, the velocity of the projectile $\beta = \frac{v}{c}$, the ionization energy I of the target material, the rest mass of the electron and a constant K [5].

For the reason that the energy loss depends on a factor $\frac{1}{\beta^2}$ it increases with decreasing particle energy but at the same time the higher the energy the higher the effective charge of the particles due to stripped of electrons. At the Bragg peak the maximum of the energy loss is reached which correspond to an energy of about 350 keV/u for a ^{12}C ion (cf. figure 2.4 on page 7).

During a real ion therapy the Bragg peak has a slight broadening to the fact of statistical fluctuations in the collisions of the single ions of the primary beam. This broadening depends on the mass of the projectiles and varies with $\frac{1}{\sqrt{M}}$. for that reason it is smaller for heavier ions than for protons. Also the lateral spread of an ion beam, caused mainly by elastic Coulomb interactions with the target nuclei is much larger for light ions or protons then for heavy particles. Altogether ion beams show a more useful behaviour for medical treatment in comparison to photon beams, and the heavier the ions the better the behaviour fits to the requirements needed for irradiation near organs at risk in cancer therapy [4] [5].
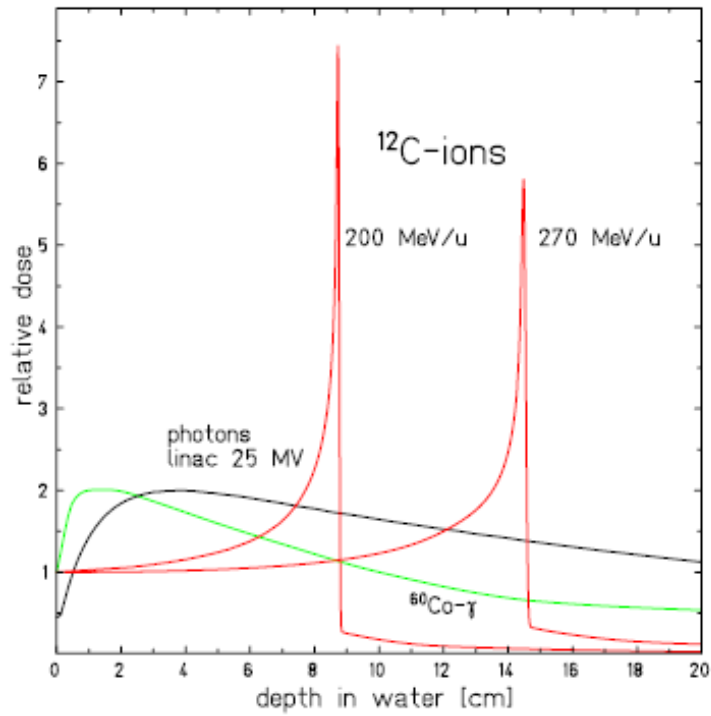
Figure 2.3: Depth-dose profiles of ^{60}Co radiation, megavolt photons, and ^{12}C ions in water [4].
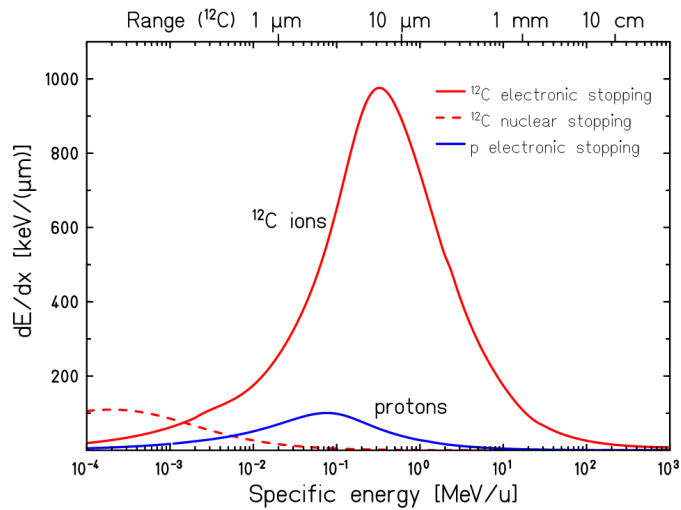
Figure 2.4: Specific energy loss dE/dx of ^{12}C ions and protons in water. The range of ^{12}C ions in water corresponding to their specific energy is indicated at the top [4].

7

3 Treatment verification in ion beam therapy

For medical issues in radiotherapy it is important to know the position and the path of the primary ion beam and the position of the Bragg peak as exactly as possible to prevent irradiation of healthy tissue. Although a few different techniques exist or at least a few promising techniques have been proposed, most of them are being investigated in fundamental pre-clinical research. All of them have to satisfy the claims needed for medical treatment which are a high accuracy combined with fast data collection and evaluation preferably directly during the daily dose delivery in radio therapy to provide the possibility to rapidly adapt the treatment [6] [7].

3.1 PET monitoring

"Positron-Emission-Tomography (PET) offers the only technically feasible method for a volumetric non-invasive verification of the ion treatment during or shortly after daily dose delivery in radiotherapy." [7] PET monitoring is based on the detection of β^+ emission which is induced by the nuclear interaction between the primary ion beam and the molecules of the irradiated tissues. This β^+ particles annihilate with electrons directly in the target and a pair of photons with an energy of 511 keV is produced in opposite direction. By detecting these photons and recalculating their origin it is possible to get the position of the primary ion beam. Depending on the primary ion beam species there are up to two mechanism of β^+ activation. While in case of a medical treatment using a primary proton beam the activation includes only target fragmentation in case of a primary carbon ion beam it includes both target and projectile positron emitting fragments.

Figure 3.1 on page 10 shows the activity of target fragments as a function of the penetration depth of a primary proton beam. Additionally the corresponding calculated dose distribution is mapped onto the plot. Apparent from a comparison of both functions the activity of target fragments doesn't deliver a signal of the Bragg peak as definite as desired. This behaviour changes for a treatment using a carbon ion beam. In this case the strongest signals of β^+ activation are produced by the most frequent positron-emitting
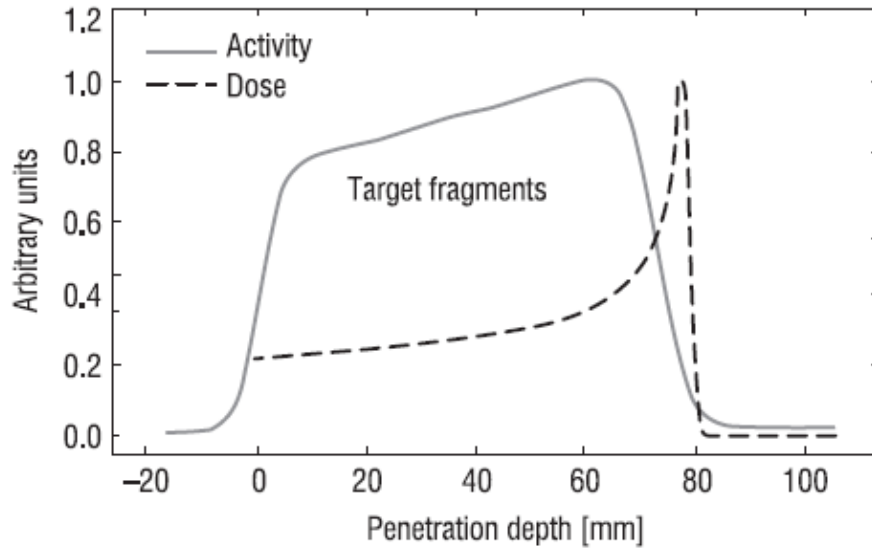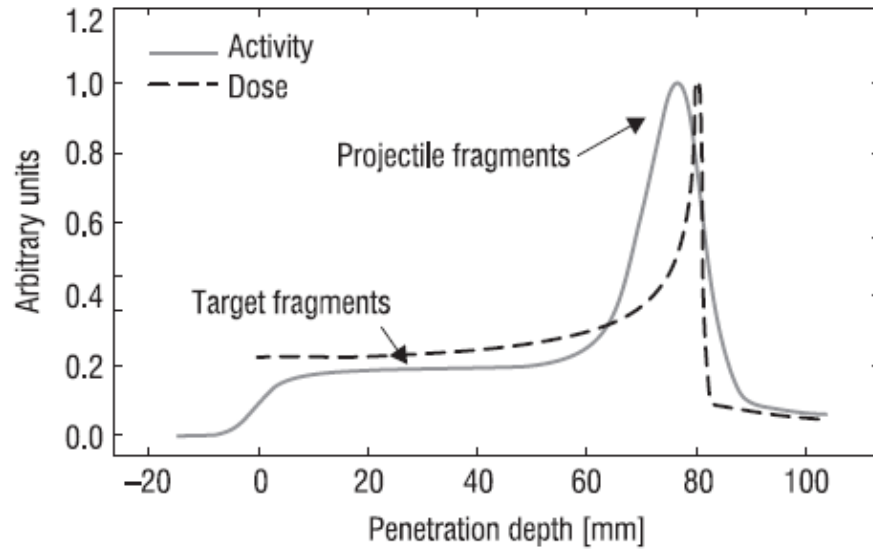
Figure 3.1: Comparison between β^+ activation and dose measured by an in-beam PET as a function of depth in a PMMA target during proton ion therapy at E = 110 MeV [7].

isotopes of the primary therapeutic ion beam, such as ^{10}C and ^{11}C from a primary ^{12}C ion beam. Figure 3.2 on page 11 contains the results of an in-beam PET measurement of the β^+ activation of a carbon ion beam as a function of the penetration depth. Again the calculated dose distribution is added for comparison. As distinct from figure 3.1 the activity has now a peak structure located shortly before the Bragg peak. The reason for the difference of these results is that activated target nuclei stay almost in the place of interaction, whereas projectile fragments are stopped and accumulated in a penetration depth expected for the defined energy of the primary ion beam.

Due to the delayed radioactive decay according to the half-live times of the typical β^+ emitting reaction products like ^{10}C, ^{11}C and ^{15}O, which range from a few seconds up to several minutes, the PET measurement can not only be performed during but also shortly after the beam delivery. For that reason so far three major clinical implementations have been developed.

in-beam PET: The 'in-beam' implementations try to acquire data during the irradiation. Although this is the only method which would allow to intervene directly during the treatment if any unexpected results occur, these installations have to deal with two major restrictions. So far the data acquisition has been only achieved between two pulses of the beam delivery because of the strong prompt radiation background during the irradiation (cf. 3.2). And the measurement is restricted to limited angle

Figure 3.2: Comparison between β^+ activation and dose measured by an in-beam PET as a function of depth in a PMMA target during carbon ion therapy at E = 212,12 MeV/u [7].

detectors with lower efficiency.

in-room PET: This means a data acquisition that starts right after the end of the therapeutic irradiation or at least just a few minutes delayed. These solutions also include on-board detectors or a full-ring scanner directly in the treatment room which is moved to the patient or vice versa. Although the data are available only after the treatment, the advantage of this method is the accurate measurement of the signal due to the use of a full ring scanner and the relatively short delay.

offline PET: Offline imaging is the technical simplest and the most economic way of realizing a PET monitoring to supervise the radiotherapy. For the data acquisition a full ring scanner installed outside of the treatment room is used. The drawbacks of this method are the long scanning time needed to compensate the loss of the short lived positron emitting isotopes and the loss of accuracy by the transport of the radioactive isotopes by physiological processes. This so called "wash-out effect" is caused by the time gap between the irradiation and the PET measurement. [7] [4]
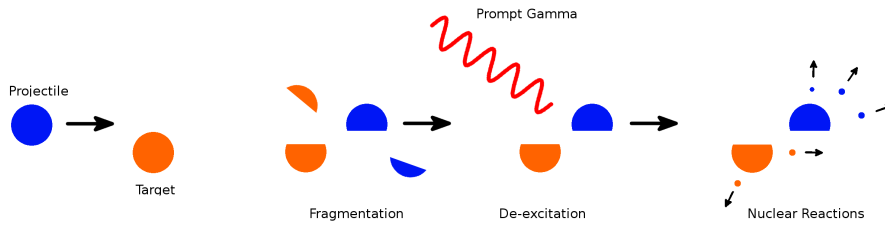
Figure 3.3: Sketch of the target fragmentation, projectile fragmentation and the emission of prompt gamma rays.

3.2 Prompt γ - photons

An alternative to PET monitoring during a radiotherapy with proton or heavy-ion beams may is the measurement of prompt photon or particle radiation. Prompt γ -rays, neutrons and other secondary particles are emitted by excited nuclei produced by the fragmentation of the projectile ions or target atoms. Figure 3.3 on page 12 shows this process which produces photons in an energy range from a few tens of keV up to 20 MeV. Since this fragmentation reactions occur along the whole stopping path of the primary ion beam it should be not only possible to measure the total dose but may also determine the distribution of the deposit dose. Unlike the method of PET monitoring which uses β^+ reactions and for this has a short but nevertheless influential time delay, the emission of prompt γ -rays typically happens within less than 1 ns after the nuclear reaction or fragmentation occurs. So if the prompt γ emission is used for monitoring, the physiological processes do not affect the measured signal and there is less disturbing prompt radiation back ground because exactly this background is used for the monitoring [4] [1].

4 GATE

4.1 GEANT4

GEANT4 is a simulation toolkit to simulate the interaction between particles and matter [8]. It contains several modules to realize a complete range of functionality like building different geometries, physics models and tracking. The physics lists and processes offered by the developer include a high range of effects like electromagnetic, hadronic and optical processes. GEANT4 can handle many different particles, elements and materials in an energy range starting from 250 eV up to a few TeV. GEANT4 has been developed to handle complex geometry and physic models and still keep it easy to adapt optimal to different fields of applications. The toolkit which is based on the programming language C++ is a result of a world wide cooperation between physicists and software engineers and has been used in many different fields of application, such as particle physics, nuclear physics, accelerator design, space engineering and medical physics [8].

4.2 GATE

GATE (GEANT4 Application for Tomographic Emission) is developed by the OpenGATE collaboration [9] and is based on the libraries of GEANT4 to permit a modular and versatile simulation toolkit for nuclear medicine [10]. Monte Carlo simulations are an important instrument for developing and optimizing tomographic methods in radiotherapy and GATE submit the description and simulation of dynamic systems under realistic conditions. It consequently allows to simulate many different source, detector and target constellations such as positron emission tomography (PET), single photon emission computed tomography (SPECT) and computed tomography (CT).

4.3 Building A Simulation

This section will show the main steps which have to be taken to build up an simulation in GATE for radiotherapy [11].

Material Database

To define the properties of the materials used in a specific GATE simulation a database must be called in the simulation which contains al the necessary informations. The OpenGate collaboration already supplies such a listing of materials in a file as part of GATE which includes all materials needed for the following investigations. The physical properties of atoms, molecules and compounds are defined by structures called elements and materials contained in the database. As distinct from Geant4, GATE does not use isotopic abundances because they are not important in the low to mid energy physics like radiotherapy. To call a material database the command `/ gate / geometry / setMaterialDatabase` followed by the path of the database is used [11].Below are examples for database entries.

Listing 4.1: Examples of the code of different elements and materials included in the material database of GATE [9]

```
[Elements]
Hydrogen:   S= H   ; Z=  1. ; A=   1.01  g/mole
Oxygen:     S= O   ; Z=  8. ; A=  16.00  g/mole

[Materials]
Vacuum: d=0.000001 mg/cm3 ; n=1
        +el: name=Hydrogen ; n=1
G4_WATER: d=1.00 g/cm3; n=2 ; state=liquid
        +el: name=Hydrogen ; n=2
        +el: name=Oxygen; n=1
```

Defining a geometry

When starting to set up a simulation in GATE the only existing volume is called *world*, whose dimensions need to be specified. All new volumes needed for the simulation have to be defined as a "daughter" of another volume or at least of the *world* by using the command `/ gate / "mother volume name" / daughters / name`. The new volume is always positioned relative to the center of the mother volume and must be completely inside of its mother. There exist many commands to build volumes in every needed shape and the physical properties of the volume must be set by using the material database [11].

Defining physics processes

To activate the requested physics processes for the simulation it is necessary to enable them for the specific particles by using the command `/gate/physics/addProcess [Process] [Particle]`. Then you can define energy cuts and specific models to use for the process. There are also some typical physics lists provided by the OpenGate collaboration. These lists are available in the installation directory of Gate and for the investigations in this master thesis the so called *hadrontherapyStandardPhys.mac* was used as recommended for hadrontherapy with standard processes [11].

Actor and output management

Actors are tools which can collect information during the simulation and can also modify the behaviour of the simulations. They must be attached to a certain volume of the geometry to set the location where the data are collected and they can additionally be equipped with filters to reduce the variance of collected information or specialize the data. Filters are implemented on particle type, particle ID, energy, direction and daughter volumes. There are various different actors provided by GATE and the following list just gives an expression of some of the actors used in the following investigations [11].

Simulation Statistic Actor: It counts some statistical values like the number of events, hits and tracks of the simulation or the volume it is attached to.

Dose measurement: With the help of the *Dose Actor* it is possible to record and store 3D images of the energy deposit, dose deposit, number of hits in a volume and the uncertainty of this values as well as the squared dose or energy. The collected information can be normalized and a water equivalent dose can be calculated before the data get saved in one of the submitted file types like ASCII file (.txt), root file (.root), Analyze (.hdr/.img) or MetaImage (.mhd/.raw).

Kill track: The *Kill Actor* modifies the simulation by killing the tracks or particles which interact in or leave the volume. The output is the number of tracks killed and is stored in an ASCII file

Energy spectrum: The *Energy Spectrum Actor* records various histograms for the initial kinetic energy of each track, the energy deposition per event and the energy deposition and energy loss per track. It is possible to specify the boundaries and the binning of the energy spectrum as well as the parameters of the energy loss histogram.

Production and Stopping Actor: This Actor records the production and stopping position of particles in a 3D image. For this reason it is necessary to set the required resolution after attaching the actor to a volume. Since the actor simply counts the number of all produced and stopped particles but as all of the other actors does not distinguish between particle types, an additional particle filter is recommended for most of the simulations.

Number of particles entering volume: The *Particle In Volume Actor* counts the number of particles produced outside of the actor volume and interacting in the volume. Also this actor can be separated into voxels so each particle is counted in each voxel it is interacting. Important is that a particle which passes through the volume without interaction will not be recorded.

Initialize the simulation

The initialization triggers the calculation of the cross sections, so after this step the physics list can not be modified any more and it is not possible to change the geometry by adding new volumes or vary the used materials [11].

Creating a source

A Gate simulation can handle several independent sources so for each source all necessary parameters must be set individually. The user has to define the type of the source, the type of the produced particles, the energy or energy distribution of the produced particles, the angular distribution of the emitted particles, the shape of the source or the shape of the produced beam and the placement of the source [11].

Random generator

Before starting the simulation its important to adapt the parameters for the random generator since GATE is a Monte Carlo tool and the results are depending highly on the performance of the generator. There are three different engines available in GATE and by default the Mersenne Twister is activated. While its not necessary to change this one, its important to change the default generator seed, which otherwise will remain the same for each simulation started. Using the command `/gate/random/setEngineSeed auto` is the easiest way to solve this problem [11].

Starting the simulation

The last step to take is to start the simulation. Therefore it is necessary to define an ending condition for the simulation. The solution used in this work was to specify the total number of primary particles by using the command

`/gate/application /setTotalNumberOfPrimaries [N]`.

Afterwards to start the simulation the following command was used.

`/gate/application/start` [11].

5 Simulations

5.1 Photon scattering

The objective of this work was to investigate the use of prompt γ rays for monitoring issues in hadron therapy and for that reason it was necessary to proof some required conditions. The following sides describe simulations which have been performed to verify the accuracy of the simulation tool on the one side and on the other side to check the usefulness of prompt γ rays which passed through a human body for a computer monitoring. For this reason the mean free path length of these photons as well as the scatter behaviour and the attenuation of a photon beam were studied.

5.1.1 Mean free path length of photons

The mean free path is the average distance travelled by a moving particle between two impacts which modify its direction or energy. As mentioned before one of the first investigations made, was a simulation to determine the mean free path length of photons in water. As shown later these results could be used to verify the validity of the used Monte Carlo tool.

The used virtual experimental assembly for this verification was a geometry which became the standard setting for most of the simulations executed as part of this thesis. In this setting the target for the beam was a solid cylinder with a radius of 30 centimetres and a height of 200 centimetres. Different substances were used as materials, but the most important and the most used substance in this work was G4_Water. The source of the primary particle beam was positioned slightly outside of the front of the cylinder with a gap of 10 centimetre and the produced beam passed the cylinder right through its axis (cf. figure 5.1 on side 20). In this case the source provide a beam of mono energy photons with a radius of 0.001 mm (cf. listing 5.1 on side 20) whereby the energy was changed for succeeding simulations to determine the mean free path for different photon energies.
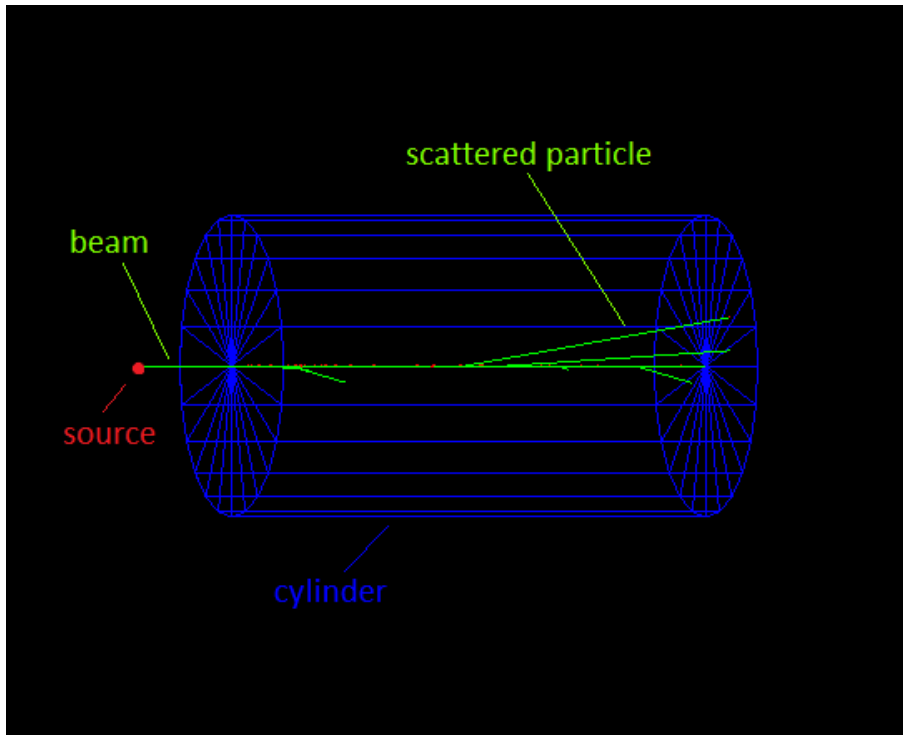
Figure 5.1: Experimental setup for the simulation of the mean free path of photons.

Listing 5.1: Gate code to define the source to investigate the mean free path of photons

```
/gate/source/singlegamma/setActivity 1. becquerel
/gate/source/singlegamma/gps/particle gamma
/gate/source/singlegamma/gps/energytype Mono
/gate/source/singlegamma/gps/monoenergy {primaerenergie} MeV
/gate/source/singlegamma/gps/type Beam
/gate/source/singlegamma/gps/shape Circle
/gate/source/singlegamma/gps/radius 0.001 mm
/gate/source/singlegamma/gps/centre -110. 0. 0. cm
/gate/source/singlegamma/gps/direction      1 0 0
```

The last missing parts of the simulation setup were the used actors which determine the parameters and informations collected during the virtual experiment. For this special problem a combination of two actors, namely a *Kill Actor* and a *Particle In Volume Actor* as shown in listing 5.2 on side 21 was used. This *Particle In Volume Actor* detects all particles in a specific volume which interacts in any way in this volume. And it does not only count all the interacting particles, it is also possible to program a desired

resolution so the particles are counted in dependence on their covered distance. But the problem was to only take into account the first interaction of every photon. For this reason a *Kill Actor* was set up which as the name says, killed every particle which interacts in his desired volume. It is important that it kills the particle right after the first interaction in the volume, so no secondary particles are produced, but the *Particle In Volume Actor* recognize this interaction. So every time a new photon passed the target and got absorbed or scattered, the actors counted the particle and prevented all future interactions by deleting the particle.

Listing 5.2: Gate code to define the actors to investigate the mean free path of photons

```
/gate/actor/addActor KillActor          Killer
/gate/actor/Killer/save                 Output/Killer.txt
/gate/actor/Killer/attachTo             Phantom

/gate/actor/addActor ParticleInVolumeActor  Weglaenge
/gate/actor/Weglaenge/save
                        Output/Weglaenge{primaerenergie}.txt
/gate/actor/Weglaenge/attachTo          Phantom
/gate/actor/Weglaenge/setResolution     1 1 4000
/gate/actor/Weglaenge/stepHitType       post
/gate/actor/Weglaenge/addFilter         IDFilter
/gate/actor/Weglaenge/IDFilter/         selectID 1
```

So based on the used actor which was divided into 4000 voxels in beam direction and the fact that many simulation were run to get the resulting mean free path length for 100 keV steps of the primary photon energy many data were collected in terms of text files which were processed in the program Matlab. The figure 5.2 on side 22 shows the result of this first simulation of this work in a graphical way. Additional to the results also a literature value for the mean free path of photons in water is plotted in this graph to get a first impression on the accuracy of the used Monte Carlo tool.

Of course to get a quantitative result some more data were needed to match the simulation with real measurements. One possibility to get this data is to calculate the mean free path length with the help of the mass attenuation coefficient of the used material for gamma rays as the following formula shows.

$$l = (\frac{\mu}{\rho} * \rho)^{-1} \tag{5.1}$$

The necessary attenuation coefficents can be looked up in the tabular 5.1 on side 23 which
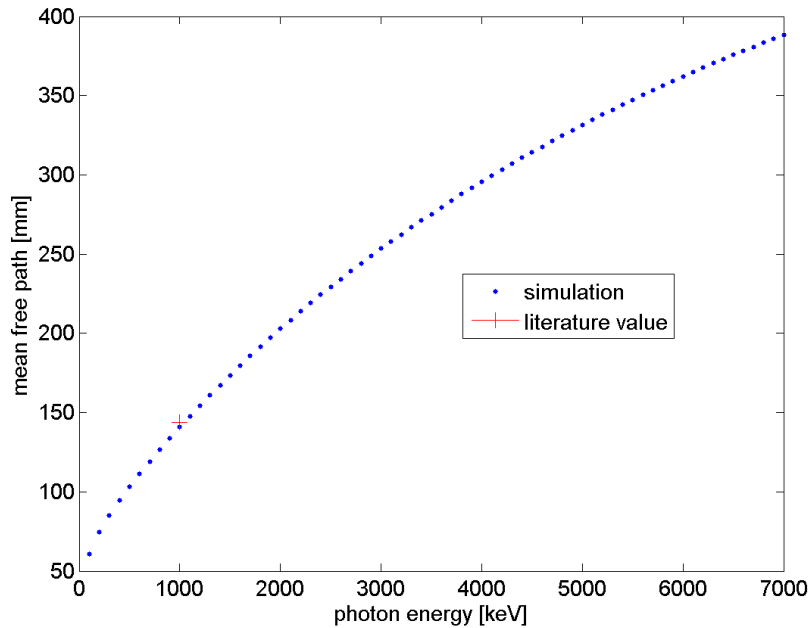
Figure 5.2: Mean free path length of photons in water simulated with GATE version 6.2.

can be found in the NIST database [12] in the internet. The plot 5.3 on side 24 again shows the mean free path but this time additionally the calculated values are mapped. As the data show the mean observational error for this simulation is about 0.7 percent which mean that the simulation is sufficient accurate.

Due to the fact that GATE is a widely used tool for Monte Carlo Simulation in the radiotherapy there exist many different physics lists and as mentioned before, it is always possible to change, activate and deactivate different physical effects. If not explicitly mentioned all the simulations used the official and so called hadrontherapyStandardPhys.mac physics list. To make sure that all the important physical effects are taken into account the previous simulations were repeated with different extended physics lists. One example was a simulation with activated Rayleigh scattering by adding the needed code to the used physics list.

Listing 5.3: Gate code for activating Rayleigh Scattering

```
/gate/physics/addProcess RayleighScattering
/gate/physics/processes/RayleighScattering/setModel
                                        PenelopeModel
```

The figure 5.4 on page 25 shows the comparison between this result and the standard

Energy (MeV)	μ/ρ (cm^2/g)	μ_{en}/ρ (cm^2/g)	Energy (MeV)	μ/ρ (cm^2/g)	μ_{en}/ρ (cm^2/g)
1.00000E-03	4.078E+03	4.065E+03	1.00000E+00	7.072E-02	3.103E-02
1.50000E-03	1.376E+03	1.372E+03	1.25000E+00	6.323E-02	2.965E-02
2.00000E-03	6.173E+02	6.152E+02	1.50000E+00	5.754E-02	2.833E-02
3.00000E-03	1.929E+02	1.917E+02	2.00000E+00	4.942E-02	2.608E-02
4.00000E-03	8.278E+01	8.191E+01	3.00000E+00	3.969E-02	2.281E-02
5.00000E-03	4.258E+01	4.188E+01	4.00000E+00	3.403E-02	2.066E-02
6.00000E-03	2.464E+01	2.405E+01	5.00000E+00	3.031E-02	1.915E-02
8.00000E-03	1.037E+01	9.915E+00	6.00000E+00	2.770E-02	1.806E-02
1.00000E-02	5.329E+00	4.944E+00	8.00000E+00	2.429E-02	1.658E-02
1.50000E-02	1.673E+00	1.374E+00	1.00000E+01	2.219E-02	1.566E-02
2.00000E-02	8.096E-01	5.503E-01	1.50000E+01	1.941E-02	1.441E-02
3.00000E-02	3.756E-01	1.557E-01	2.00000E+01	1.813E-02	1.382E-02
4.00000E-02	2.683E-01	6.947E-02	1.25000E+00	6.323E-02	2.965E-02
5.00000E-02	2.269E-01	4.223E-02	1.50000E+00	5.754E-02	2.833E-02
6.00000E-02	2.059E-01	3.190E-02	2.00000E+00	4.942E-02	2.608E-02
8.00000E-02	1.837E-01	2.597E-02	3.00000E+00	3.969E-02	2.281E-02
1.00000E-01	1.707E-01	2.546E-02	4.00000E+00	3.403E-02	2.066E-02
1.50000E-01	1.505E-01	2.764E-02	5.00000E+00	3.031E-02	1.915E-02
2.00000E-01	1.370E-01	2.967E-02	6.00000E+00	2.770E-02	1.806E-02
3.00000E-01	1.186E-01	3.192E-02	8.00000E+00	2.429E-02	1.658E-02
4.00000E-01	1.061E-01	3.279E-02	1.00000E+01	2.219E-02	1.566E-02
5.00000E-01	9.687E-02	3.299E-02	1.50000E+01	1.941E-02	1.441E-02
6.00000E-01	8.956E-02	3.284E-02	2.00000E+01	1.813E-02	1.382E-02
8.00000E-01	7.865E-02	3.206E-02			

Table 5.1: Mass attenuation coefficients for photons of different energies in water. (The data are taken from the Nist database [13].)
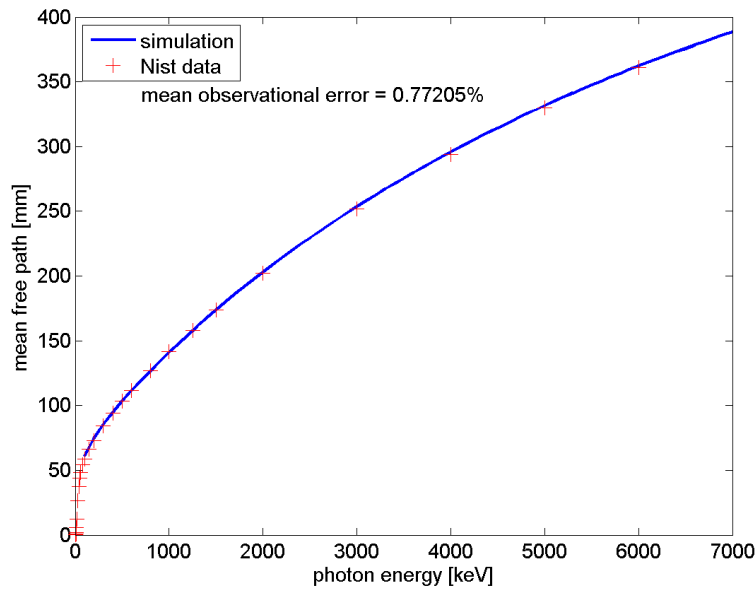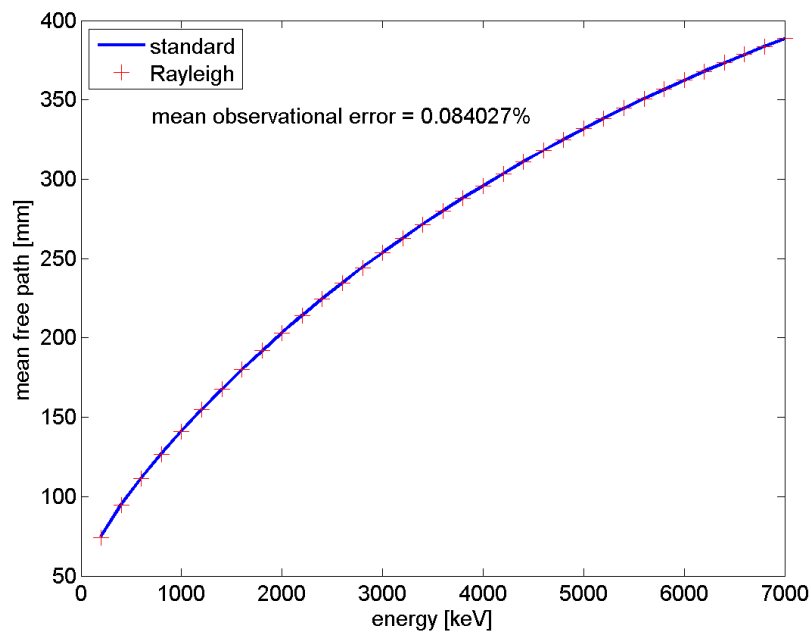
Figure 5.3: Comparison of the simulated and calculated mean free path length of photons in water. The calculated values are based on the values of the Nist database [13]

simulation. As noticeable the received error is negligible, but the needed computation time increased measurable. From that time on all the simulations performed for the whole project used the hadrontherapyStandardPhys.mac physics list to save computer resources on the one hand and to ensure comparability between the results of different simulations performed by the project team.

Since the human body consists of about over 70 percent water, the results of the previous investigations should describe the behaviour of photons passing the human body quite well. Nevertheless it was necessary to prove the consistency of the given conclusion. For comparison this kind of simulations were executed for different other materials as mentioned before. The figure 5.5 on side 25 illustrates the respective mean free path of photons, passing the different materials used. Concretely the build-in material data of GATE for adipose, brain, lung, skull and for comparison water were used. As expected the higher the energy of the photons, the higher the mean free path length. On the other side this simulations show that the higher the density of the passed materials the lower the mean free path length of the photons.

Finally the first result of this investigations is that the simulation tool works quit accurate. The more important second result is, that for the interesting energy range of the photons from about 2.3 MeV to 6 MeV, which will be described later on, the mean

Figure 5.4: Comparison of the simulated mean free path lengths of photons in water with and without activated Rayleigh scattering.
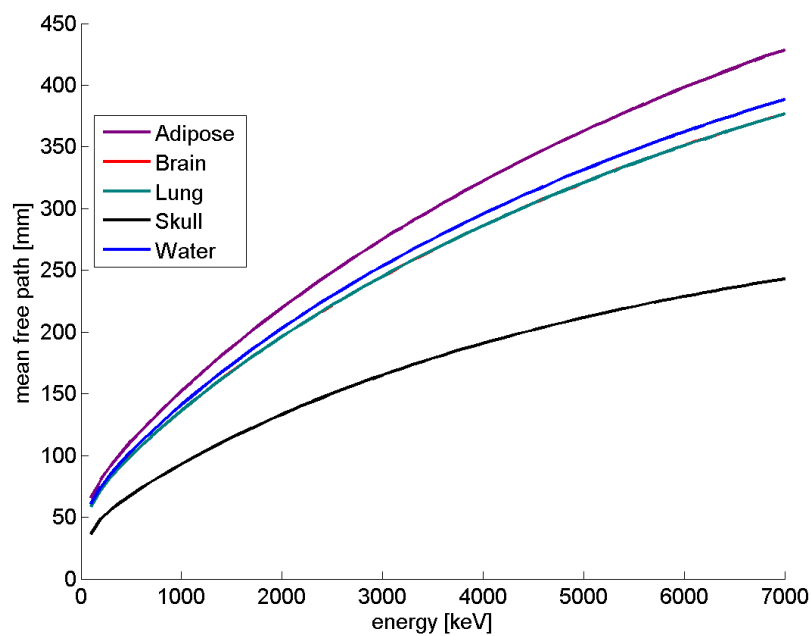
Figure 5.5: Comparison of the simulated mean free path lengths of photons in different materials.

free path seems to be long enough to detect sufficient unscattered photons outside of an irradiated tissue during an radiotherapy. Because even in a very dens material like the human skull the photons of that energy range have a mean free path of at least 12 to 25 centimetres what would be quit long in an realistic treatment. In other tissue the mean free path length is even longer.

5.1.2 Photon scattering

Beside the mean free path length of photons it is also interesting to quantify the shape of a photon beam, which is passing through the typical materials of a human body and to inspect the possibility to calculate the origin of detected photons after they have departed the irradiated issues. For this reason in the following investigations again a photon beam passing a specific material was simulated, but this time the measurement of the scattering and the absorption had priority.

Based on the available computing time, and the capacity to evaluate the resulting data, it was not possible to perform as many simulations as before to calculate the mean free path length. Instead of dividing the former energy range into 100 keV steps again, it was necessary to limit the simulations to some specific photon energies. The photon energies used in the following simulations were based on a diploma thesis which investigated on the energy spectra of prompt γ rays of materials irradiated by a carbon ion beam [6]. Some of the important results of this thesis are shown in figure 5.6 on side 27. The data were obtained by simulations with GATE version 6.1 and show the production of photons during the irradiation of a water target by a carbon ion beam. On the X-axis the energy of the produced photons is plotted while the Y-axis represents the count rates. The data indicate that on the one side the primary energy of the carbon ions influence the count rates, discernible on the different count rates for the different coloured curves for the diverse carbon ion energies. On the other side the basic behaviour of the energy spectra remains the same for all primary energies so all the prominent peaks are at the same energy value and have a similar ratio to each other.

To save computing time and capacities the focus for the investigations on the photon scattering was on this prominent peaks, enumerated in tabular 5.2 on side 27. For the following investigations the basic geometry remained unchanged. Again a photon beam with a radius of 0.001 mm penetrated a cylindrical target with a radius of 30 centimetres and a length of 200 centimetres build up by G4_Water, as shown in the previous figure 5.1 on side 20 as well as the same hadrontherapyStandardPhys.mac physics list as before. But the used actors and their placement and for that reason the collected data were different. For the designated target to map the profile of the photon beam as well as the scattered photons it was necessary to run several simulations, in concrete terms for every of the
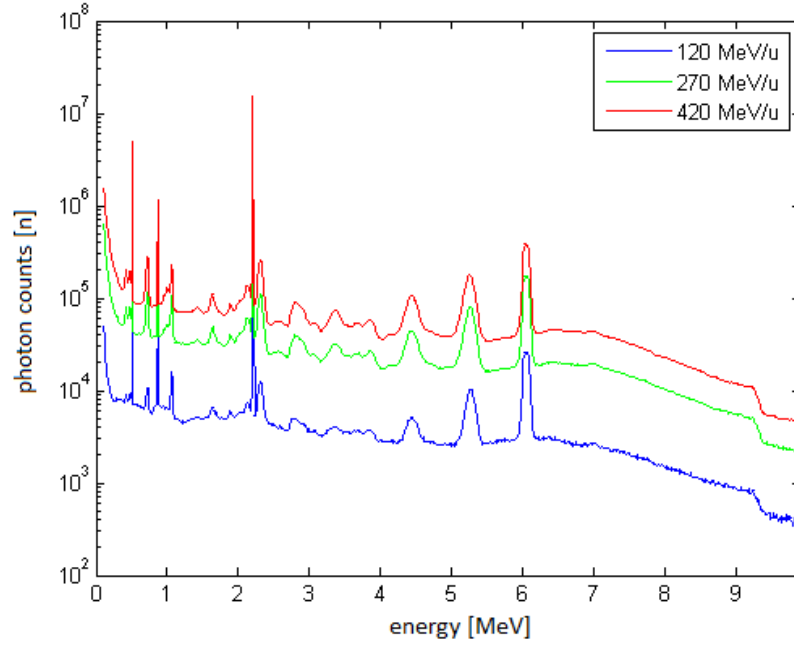
Figure 5.6: Energy spectra of prompt gamma emission in a water target irradiated by carbon ion beams of various energies. The graph shows the counts of emitted photons as a function of their energy. [6]

0.511 MeV	2.3 MeV
0.85 MeV	4.5 MeV
1.1 MeV	5.2 MeV
2.2 MeV	6.1 MeV

Table 5.2: Prominent peaks of the energy spectra of prompt gamma rays emitted by water irradiated by a carbon ion beam [6]
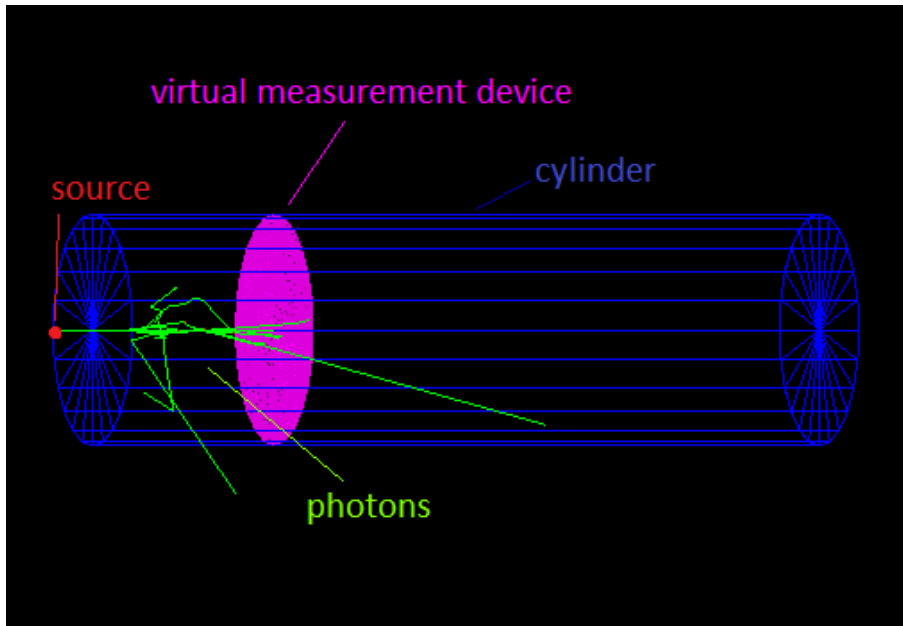
Figure 5.7: Experimental setup for the simulation of the scattering of photons

prominent peaks of the energy spectra and for various penetration depth of the photon beam. The virtual measurement device was realised by an additional thin slice composed of many rings, which was brought into the water target in the respective distance as shown in figure 5.7 on side 28 and a system of numerous actors, attached to the particular parts of the slice. The listing 5.4 on side 28 contains the code for one piece of the measurement slice and the associated actor.

Listing 5.4: Gate code for the used virtual measurement device to investigate the photon scattering

```
/gate/Phantom/daughters/name detector_100_0
/gate/Phantom/daughters/insert cylinder
/gate/detector_100_0/geometry/setRmin 0 mm
/gate/detector_100_0/geometry/setRmax 0.5 mm
/gate/detector_100_0/geometry/setHeight 0.01 mm
/gate/detector_100_0/placement/setTranslation 0. 0. -900. mm
/gate/detector_100_0/setMaterial G4_WATER
/gate/detector_100_0/vis/setColor magenta

/gate/actor/addActor KillActor KillActor_100_0
/gate/actor/KillActor_100_0/attachTo detector_100_0
/gate/actor/KillActor_100_0/save
```

```
                          Output/Primaerenergie_{primaerenergie}/
                          KillActor_100/KillActor_100_0.txt
/gate/actor/KillActor_100_0/addFilter particleFilter
/gate/actor/KillActor_100_0/particleFilter/addParticle gamma
```

The first part of the code builds the geometry which is used in the second part for the placement of the actual actor. In this example the code creates a slice in the centre of the axis of the cylindrical target. Because the translation is set to minus 900 mm the slice is brought in at a penetration depth of 10 cm since the whole cylinder has a length of 200 cm. The final lines of the code defines a *KillActor*. As explained before this actor deletes all the particles which pass or interact in the geometry it is attached to. Additional it counts all the deleted particles and that way collects on the one hand the interesting data, on the other hand makes sure that the photon can not be detected again by the same or an other actor in case of an afterwards backscattering.

In the complete simulation such combinations of geometry and actor were integrated for every segment from the beam and target axis till the cylinder barrel in steps of 5 mm. So with the collected data of some simulations it was possible to reproduce the shape of the beam and by then the scattered photons. For all of the simulations to study the scattering of photons the execution was made with 10^7 primary particles and it was made a simulation for every centimetre of penetration.

For the first analysis the most prominent peak of the energy spectra at about 2.2 MeV was chosen. This peak originates in the neutron capture of hydrogen cores during the irradiation of a ion therapy [6]. The plot 5.8 on page 30 shows the count rate of these 2.2 MeV photons at selected penetration depth as a function of their radial distance from the axis of the cylindrical target, which is as well the axis of the unscattered photon beam. As expected the counts of remaining unscattered photons in the axis decrease if the path through the target gets longer. This can be seen by the sized points at the left side of the plot, which mark the count rate of the remaining photon beam. For the first few centimetre a major part of the photons passes the water target without interaction. This matches with the result of the investigation on the mean free path length. Of course for higher path length the counts of unscattered particles sink as expected, but even for a penetration depth of half a meter the major part of the detected Photons remains in the previous photon beam. For this it is necessary to pay attention to the logarithmic caption of the function axis. The count rates of the scattered photons for each part of the measurement device is at least two orders of magnitude lower then the signal of the primary beam. Additional in this interpretation of the data the geometrical setup was not taken into account completely, because the outer rings of the measurement slice had a lager surface, so theoretical they should count even more particles. On the other side the required scattering angle for photons to hit the outer surfaces is smaller then for the
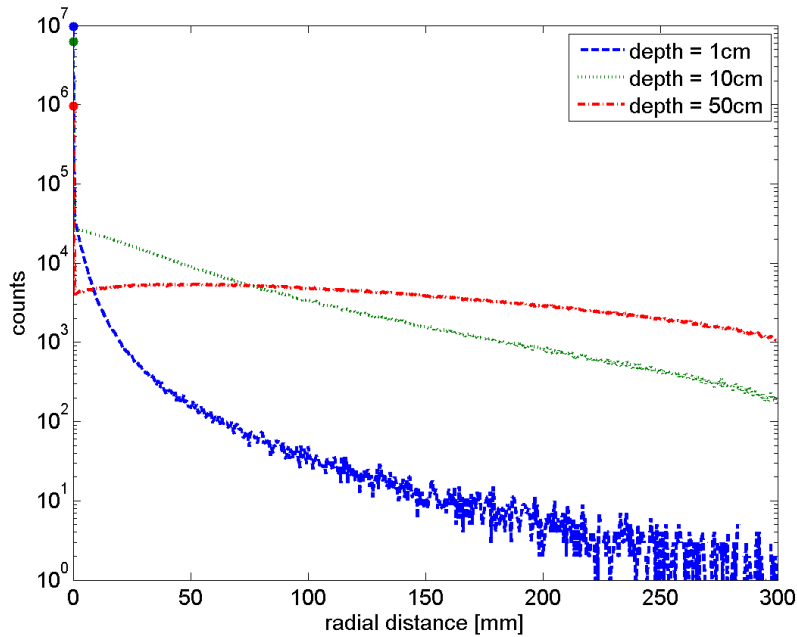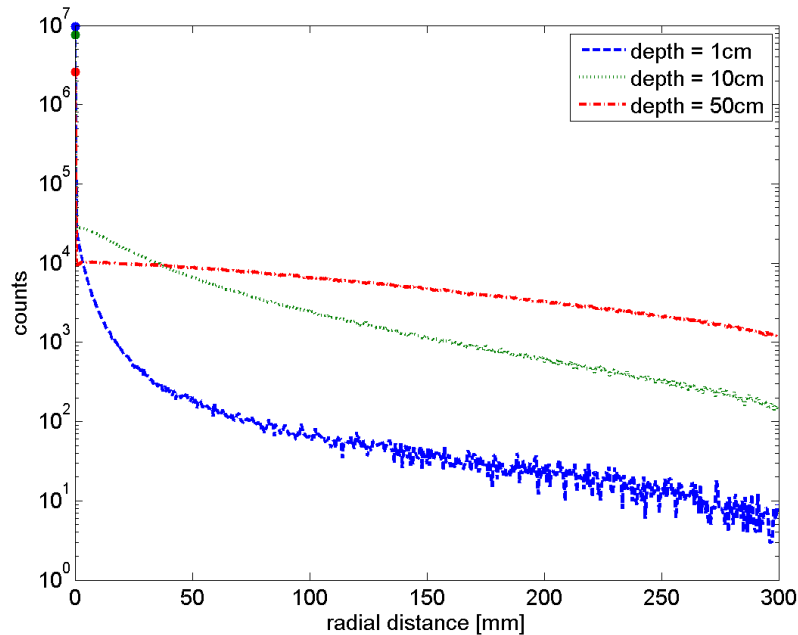
Figure 5.8: The measured scattering of 10^7 primary photons of 2.2 MeV after different penetration depths in a water target.

inner. But as long as the real scatter position is not measured and as long as there is no complete tracking for every single photon, it is not possible to determine the needed correction for this geometrical issues. Furthermore there were also photons which were scattered in a very large angle or even back scattered and for that reason could not be detected by this type of experiment. Since the gaol of this simulation was to proof if its possible to recognize the position of the primary beam after he has passed the target in a way which is workable also for real experiments the results are still valid.

As mentioned before this data were collected for all of the prominent peaks to make sure the general behaviour of the produced photons during an radiotherapy is similar. For comparison the figure 5.9 on side 31 includes the described functions for a primary photon beam with an energy of 6.1 MeV. The most obvious difference are the higher count rates for the 6.1 MeV photons at the respective penetration depth. Especially the counts of photons in the beam are more then doubled. On the other side the function for the scattered photons at a penetration depth of 10 centimetre has not increased. The reason for both effects is the increased mean free path length, which induced the smaller rate of scattering and so more photons remain in the beam axis and less photons can be detected as scattered photons. Interesting is the fact that for higher penetration depth the count rates not only for the unscattered but also for the scattered photons increase
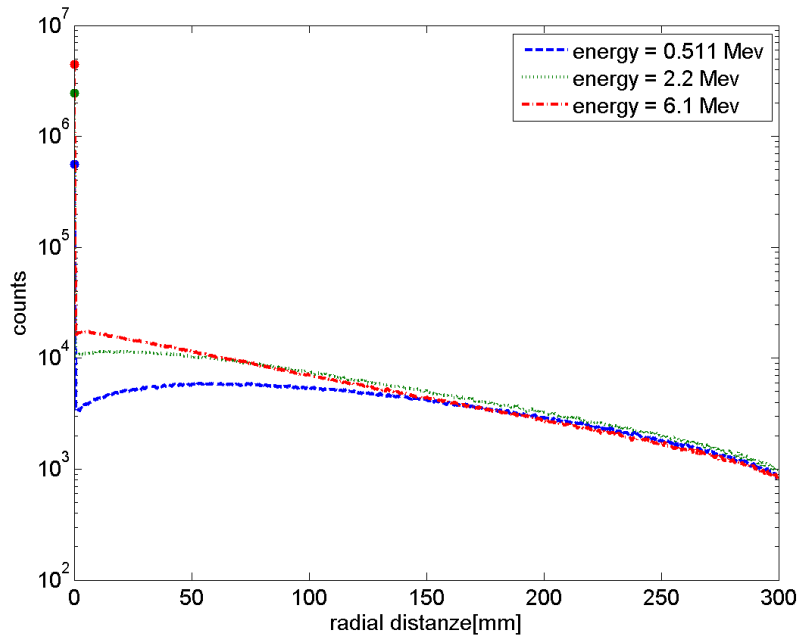
Figure 5.9: The measured scattering of 10^7 primary photons of 6.1 MeV after different penetration depths in a water taget.

compared to photons with lower primary energy. This is achieved on the one hand by the increased mean free path length, on the other hand by the decreased absorption of photons by the target material, in this case water. So the chance to detect an scattered photon is better for a higher primary energy, but this effect only carries into weight for deeper penetration depth. For the penetration depth of only one centimetre its similar. To detect photons at large distance from the axis, it is necessary that the photons are scattered in a large angle and then travel quite a long distance through the target again induced by the chosen geometrical setup. Both conditions increase the probability of the photon to get absorbed, especially for photons with lower energy as explained before.

This simulations were made for all prominent peaks and the results were always the same, so there was no unexpected behaviour for any of this energies. The functions in figure 5.10 on page 32 show the scattering of photons of different energies after passing though 30cm of the cylindrical water target. As expected after the previous results the comparison of the function and the concrete count rates shows that the single functions have the same manner. Additionally the figure again shows that for the reason of a higher primary energy more photons remain unscattered in the axis of the beam and at the same time by the decreased absorption more scattered photons are detected. For lower energies the photons are scattered more often, but this scattered photons are also absorbed by
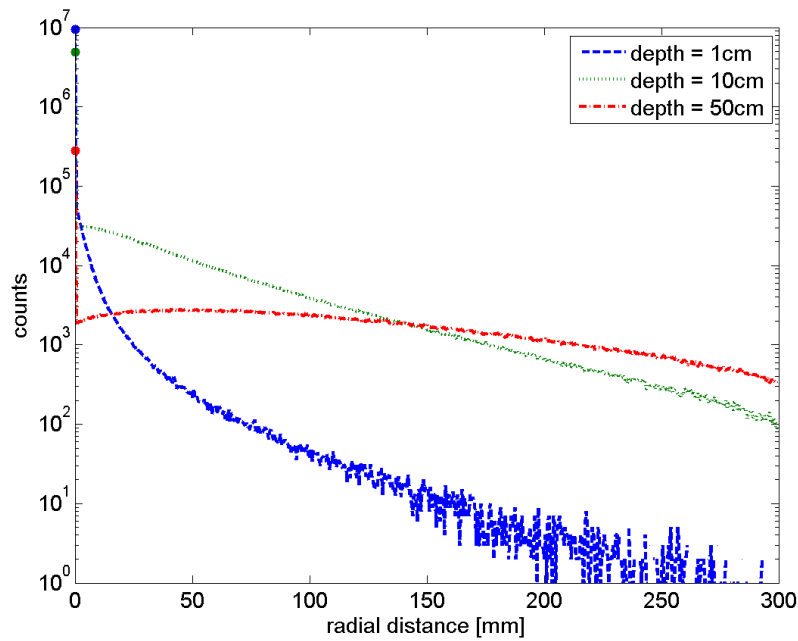
Figure 5.10: The measured scattering of 10^7 primary photons for some primary energies. The data were collected in a water target in a depth of 30 cm.

the material with higher probability. As a result of this two effects the signal of the scattered photons in this simulations is independent of the primary energy always at least two orders of magnitude smaller than the signal of the residual beam.

Finally simulations to proof this conclusion for its validity were made with other target materials. For the already mentioned reasons and for the comparability the chosen materials were again adipose, brain, lung and skull. Figure 5.11, figure 5.12 and figure 5.13 beginning on side 33 contain the same analysis for the target material skull. Also these data result in the same conclusion as before and confirm them.

The differences between the materials can be seen in figure 5.14 on page 34 which again shows the photon scattering measured with the known geometry. The graphs illustrate the count rates of the photons as a function of the radial distance for a fixed energy of 2.2 MeV and a penetration distance of 30 cm for various materials. As expected denser materials scatter more photons so less photons remain in the axis of the primary beam. But these denser materials also absorb more photons, so the counts of detected scattered photons in this penetration depth are also lowered with the result that the signal of the beam has again an higher magnitude and provide a significant count rate. The only uncommon behaviour is displayed by the function for the target material lung. While the mean free pass in lung fits to the results of the other materials (cf. figure 5.5), the scattering
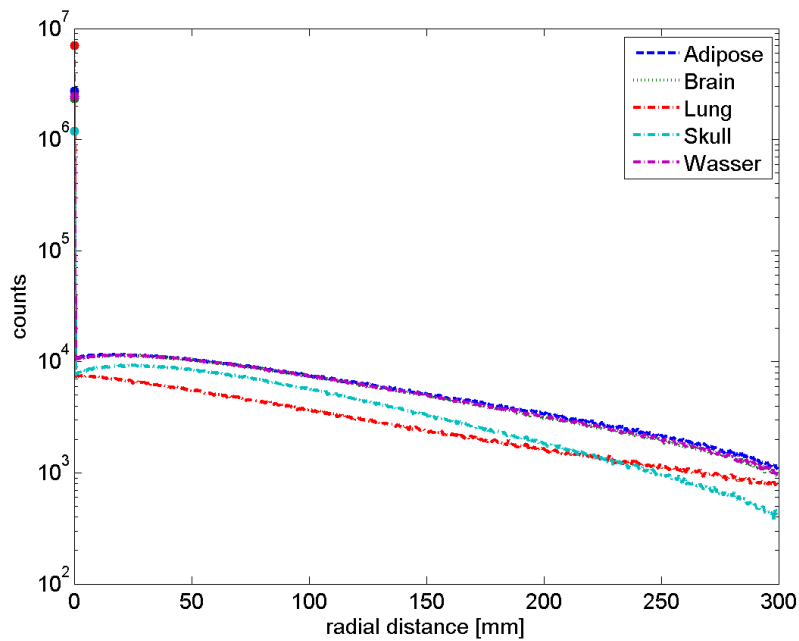
Figure 5.11: The measured scattering of 10^7 primary photons of 2.2 MeV after different penetration depths in a skull target.
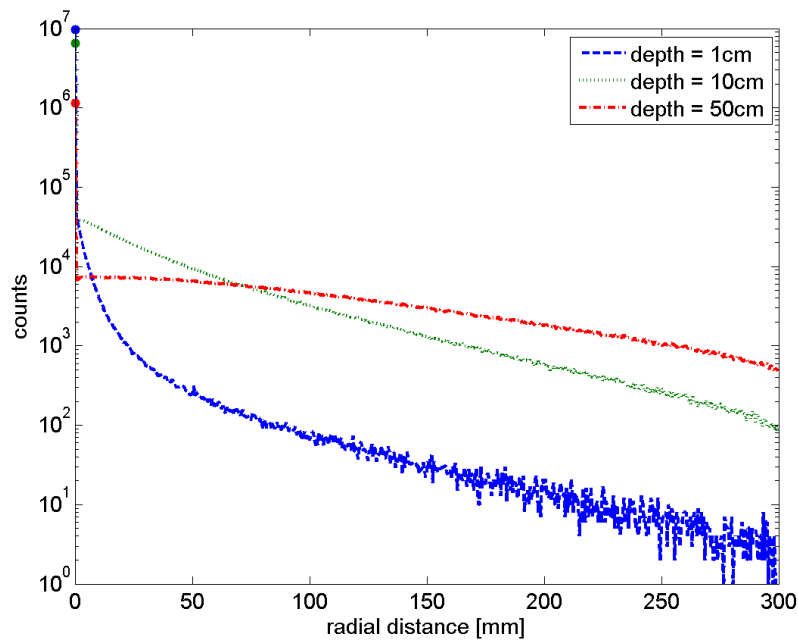

Figure 5.12: The measured scattering of 10^7 primary photons of 6.1 MeV after different penetration depths in a skull target.
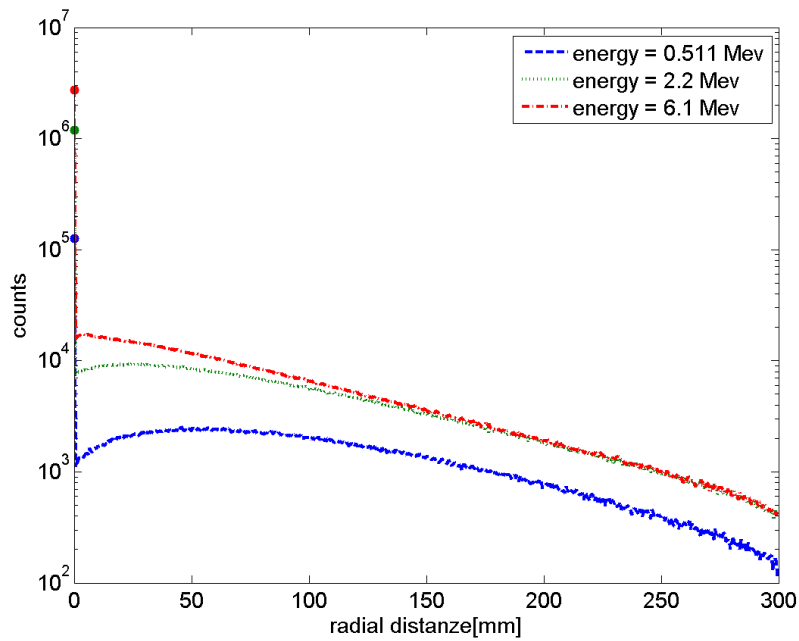
Figure 5.13: The measured scattering of 10^7 primary photons for some primary energies. The data were collected in a skull target in a depth of 30 cm.

Figure 5.14: The measured scattering of 10^7 primary photons with 2.2 MeV in a distance of 30 cm in different materials.
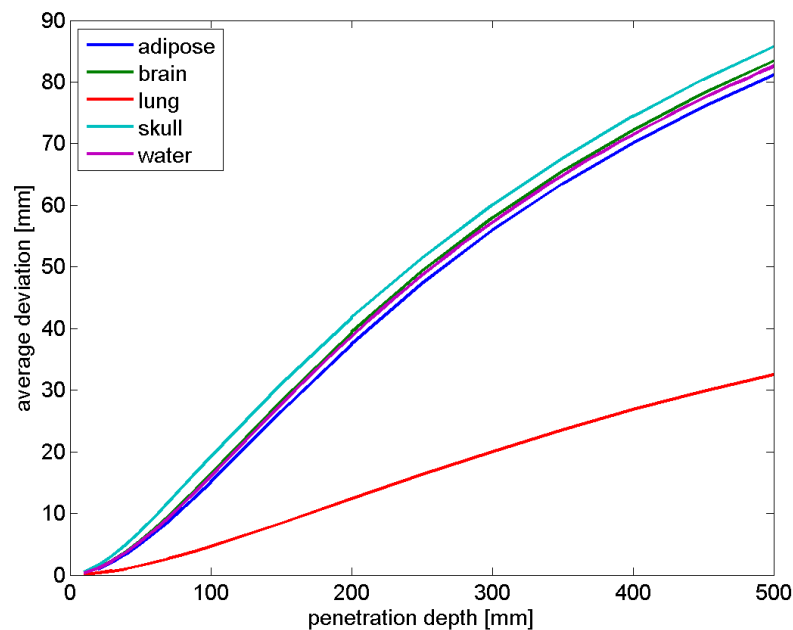
Figure 5.15: The average deviation of scattered and unscattered photons as a function of the penetration depth.

distinguishes slightly from the scatter function of the others. In lung less photons then expected were scattered out of the initial beam. The reason for this could be the material composition of lung which consist to a great part of air and therefore light particles. This low scatter rate is also the reason for the low count rate of scattered photons in lung as distinct from the scatter rate in skull, which is also lower then the others, but caused by the higher absorption rate in skull.

The figure 5.15 on page 35 summarizes the average deviation of the detected photons from the axis of the primary beam. Again the curves show a similar behaviour for the different materials except for lung which has a exceptional position for the reasons given above. The denser materials have a higher average deviation cause of their higher scatter rate. The higher absorption does not weak this effect, for the reason that also the photons in the beam are getting absorbed by a higher rate.

This investigations finally results in the conclusion that the shape of a photon beam, or the scatter manner of a single photon, which is passing through a target material, is depending on the energy of the primary photon, the penetration depth in which the measurement happens and the properties of the used irradiated material. Nevertheless the position of the beam and as a consequence the position of the source of the photons is determinable, regardless of the used material or the other used parameters.
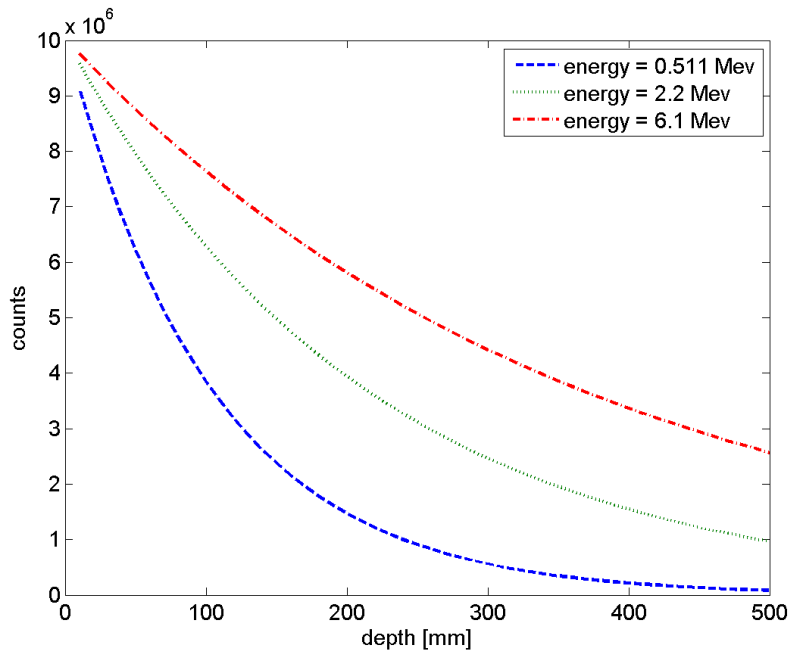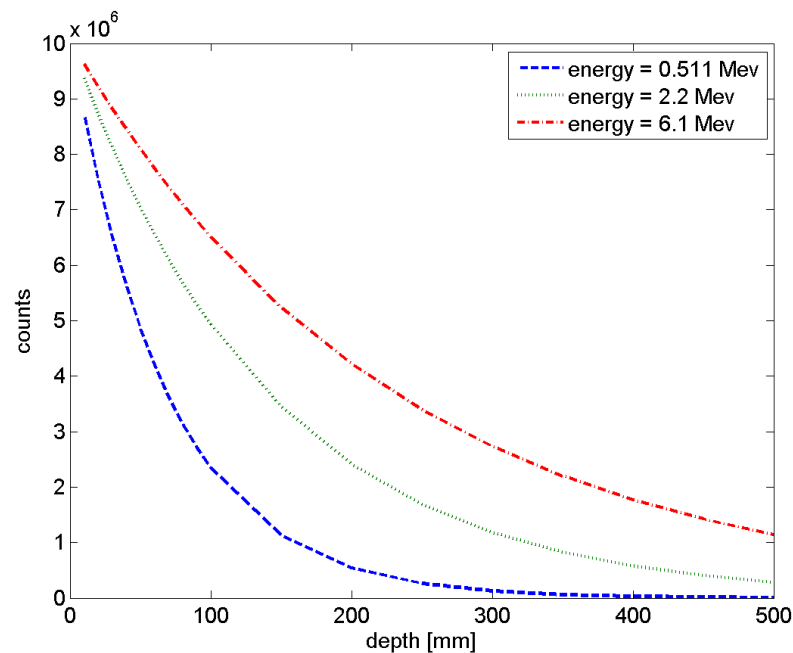
Figure 5.16: The in beam photon counts of 10^7 primary photons and various primary energies as a function of the penetration depth in a water target.

5.1.3 Attenuation of photon beams

In the former section the scattering of Photons in different materials was discussed. In many cases it is important to know as exactly as possible how this effects the measurement and the data, whereas in other cases it is more important to have an information about how strong a beam would be attenuated, and if it is possible to detect enough particles outside an irradiated target to get a statistical usable result. For this reasons the data of the presented simulations were also used to acquire knowledge about the beam attenuation. The graphs in figure 5.16 on side 36 show the count rates of detected photons in the remaining beam as a function of the penetration depth.

As expected the lower the energy of the photons the weaker the remaining detectable signal of the photon beam. But nevertheless for photons within an energy above 2 MeV the signal is quit sufficient for typical penetration depth in the ion therapy. Already for a photon energy of 2.2 MeV and a depth between 20 and 30 cm the signal is in a range of about 25 to 40 percent. For 6.1 MeV photons the remaining count rates for this range is in a area of 40 to 60 percent, and someone has to take into account that as the energy spectra for prompt gamma rays shows (cf. 5.6on side 27), many photons with even higher energies are produced during an radiotherapy with carbon ions. For lower penetration

Figure 5.17: The in beam photon counts of 10^7 primary photons and various primary energies as a function of the penetration depth in a skull target.

depths the count rates are even better. But of course the irradiated material and the material which the photons have to pass through influence the resulting signal as well. For comparison figure 5.17 on side 37 shows the same function for a virtual target made out of human skull. Apparent from these data the signal of the remaining photon beam is weaker for denser material. But even for an unrealistic target completely made out of human skull the acquired counts in a penetration depth of 200 mm for 2.2 MeV to 6.1 MeV photons were in a range of about 25 to 40 percent.

These figures only show the behaviour of the absolute count rates. Of course in a real measurement, especially if the aim is to recalculate the origin of detected photons, the scattered photons outside of the beam which are also detected have to be taken into account. So not only the count rate has to be high enough, but also the ratio of the detected unscattered photons to the scattered photons, or the totally detected photons has to be sufficient good. To illustrate the results regarding this figure 5.18 on side 38 shows the relative count rate of the unscattered photon beam for a water target. On the Y-axis the ratio of the unscattered photon counts to the totally detected photons is plotted, while on the X-Axis again the penetration depth is plotted. Again as expected the ratio is better for higher photon energies and for lower penetration depth, cause of the lower scatter rate by this conditions. The values for this investigations are quit satisfying.
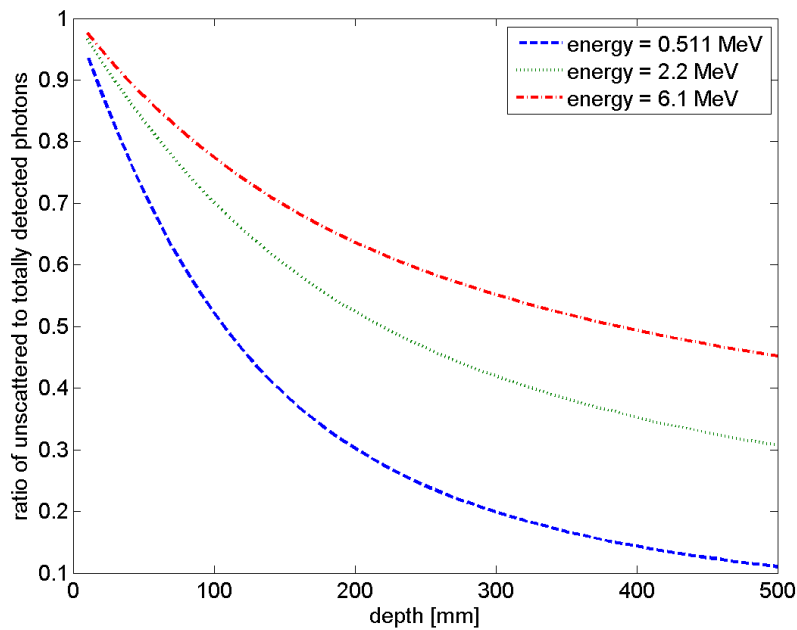
Figure 5.18: The ratio of in beam photon counts to totally detected photon counts as a function of the penetration depth in a water target.

So for a photon energy of 6.1 MeV and a penetration depth of 20 cm the ratio has a value above 60 percent, and even photons with a lower energy of 2.2 MeV and a used penetration depth of 50 cm reach a ratio above 30 percent. Figure 5.19 on side 39 shows the same function for the skull target and also here the values are quite well. In the energy range of 2.2 to 6.1 MeV and an penetration depth of 20 to 50 cm the ratio is in an area between 25 and 55 percent. Although the part of detected scattered photons overbalances, the amount of detected unscattered photons should be enough to recalculate the origin of the photons.
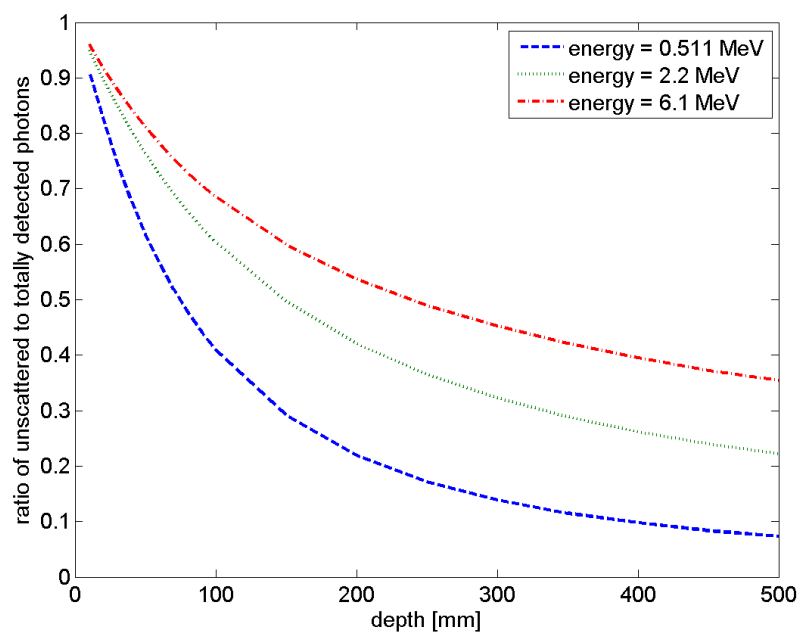
Figure 5.19: The ratio of in beam photon counts to totally detected photon counts as a function of the penetration depth in a skull target.

5.2 Photon production

The former section of this work concentrated on the behaviour of photons which passes through different materials. As mentioned the aim of the project was to check the possibility to determine the position of the Bragg peak inside of a irradiated target by the measurement of the produced gamma rays outside of the target. Since these investigations supplied results which are sufficient satisfying for the needing of this project and the possibility to calculate the origin of detected photons outside of the material it was important to collect informations about these origins of the photons. For this reason the following investigations were concerned with the production of photons during an irradiation of a target material by an ion beam. The aim was to measure the photon production as a function of the penetration depth of the carbon ion beam in a water target and find different parameters of the produced photons, which are linked to the position of the Bragg peak.

5.2.1 General investigations

First of all it was necessary to collect some first data to schedule the next steps. For that purpose the geometries respectively the parameters and actors of the former simulations again had to be slightly modified. The geometry in principle remained quit untouched. Again a solid cylinder with a radius of 30 centimetres but a height of 100 centimetres was used as a target for the primary beam. As before the target material was G4_Water. To save calculation time and resources this simulations were not made for other target materials. The main difference between the former investigations and the simulations in this section was the different source for the primary beam. Still the source was positioned slightly outside of the cylinder so the produced beam only had to overcome a gap of 10 centimetre before it had to pass the target cylinder along its axis. But in contrast to the simulations in section 5.1 the source produced a carbon ion beam with the shape of a circle and a radius of one millimetre. So the photons which are interesting this time were produced by the interactions of the carbon ions of the primary beam with the target material. Listing 5.5 contains the GATE code for the used sources, whereby the different primary energies were controlled by a entry which replaced the placeholder {primaerenergie}. The number of the primary ions remained 10^7 particles for all of the simulations presented in this section. Figure 5.20 on page 41 shows the geometry of the setting which is quit similar to the previous simulation settings.
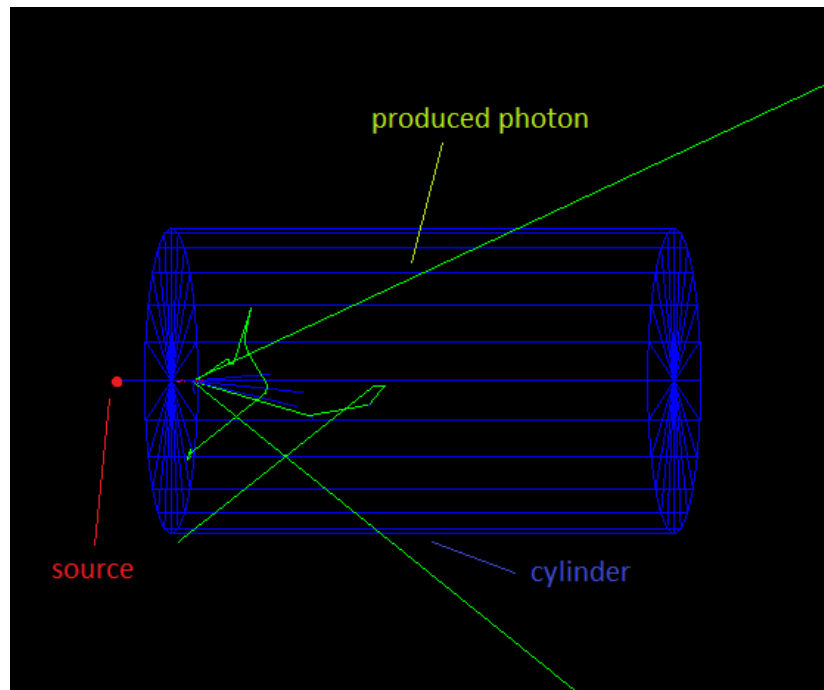
Figure 5.20: Experimental setup for the first investigations on the photon production during an carbon ion therapy.

Listing 5.5: Gate code for a carbon ion beam source for investigations on the produced photons during a radiotherapy

```
/gate/source/addSource    C12      gps
/gate/source/C12/gps/particle        ion
/gate/source/C12/gps/ion             6 12 +6 0
/gate/source/C12/gps/energytype      Mono
/gate/source/C12/gps/monoenergy      {primaerenergie} MeV
/gate/source/C12/gps/pos/type        Beam
/gate/source/C12/gps/pos/shape       Circle
/gate/source/C12/gps/pos/radius      1.0 mm
/gate/source/C12/gps/pos/centre      0.0 0.0 -60.0 cm

/gate/source/C12/gps/direction       0 0 1
```

The measurement itself was realized by a so called *Production And Stopping Actor*. This actor counts all particles produced and stores the result in one of the two generated output file and all stopped or killed particles in the other output file. Of course also this

actor has to be linked to a part of the geometry of the simulation, and as for the other actors, also for this one exists a couple of helpful options and filters to adept the actor to the respective requirement of the measurement. Listing 5.6 shows the used actor for a first investigation on the produced gamma rays during a radiotherapy. The actor was attached to the part of the geometry called *Phantom* which labeled the cylindrical target for the ion beam. The *setResolution* option is a possibility to voxelize the volume of the actor to get a higher resolution without the need to build a real detection device with the respective resolution and without the need to attach a own actor to every part of this geometry. The last parameters of the code for the *Production And Stopping Actor* limited the detected particles by a simple filter. So for the following investigations only the produced photons were detected for a resolution of 1 millimetre in direction of the beam axis.

Listing 5.6: Example code for a Production And Stopping Actor used for investigations on the produced photons during a radiotherapy

```
/gate/actor/addActor ProductionAndStoppingActor  Gamma_ges
/gate/actor/Gamma_ges/save
        Output/Primaerenergie_{primaerenergie}/Gamma_ges.txt
/gate/actor/Gamma_ges/attachTo      Phantom
/gate/actor/Gamma_ges/setResolution 1 1 1000
/gate/actor/Gamma_ges/stepHitType   post
/gate/actor/Gamma_ges/addFilter particleFilter
/gate/actor/Gamma_ges/particleFilter/addParticle gamma
```

This simulations was performed for different primary carbon ion energies in a range between 1440MeV and 4800 MeV to collect the interesting data for typical energies in radiotherapy respectively in the typical energy range of the future treatments at Med Austron. As the data of the former simulations also these were processed with Matlab and worked up in a graphical way. The figure 5.21 on page 43 shows the results of three selected simulations with an energy of 1440 MeV, 2880 MeV and 4800 MeV of the primary carbon ion beam. The vertical lines in the same colour as the functions mark the Bragg peak for the given situation. As can be seen from the figure the count rates for produced photons increase in the area of the Bragg peak compared to the expected curve of the function. However it is also apparent from the graphs that for higher primary energies of the carbon ions the signal of the Bragg peak is not as significant as for the lower ion energies. So it is important to improve the significance by finding further or more specific parameters, not only for the high primary energies but for the complete energy range to enable the calculation of the position of the Bragg beak by measuring these photons
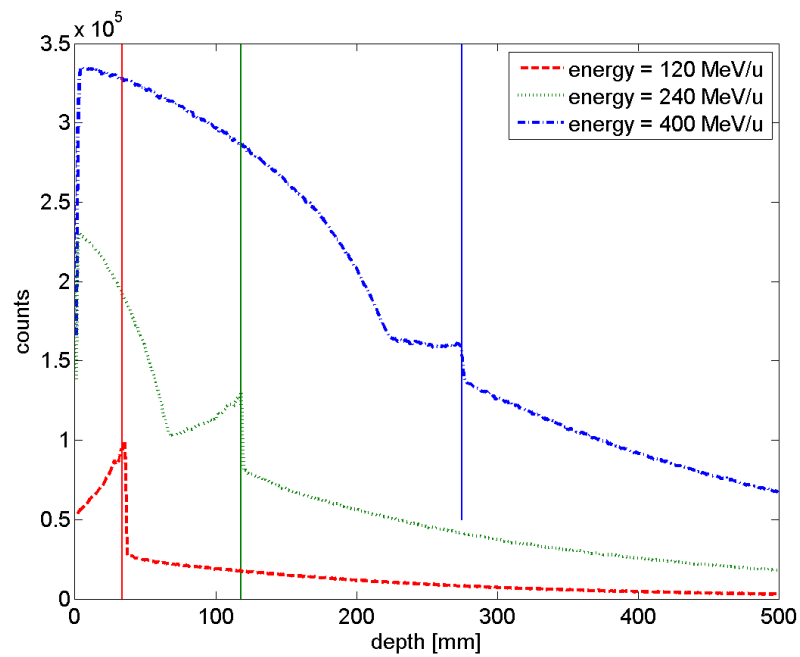
Figure 5.21: Selected photon productions for a water target irradiated by a carbon ion beam as a function of the penetration depths. The graphs show three different primary energies of the carbon ion beam which are in a typical medical energy range and are simulated with 10^7 primary particles [14].
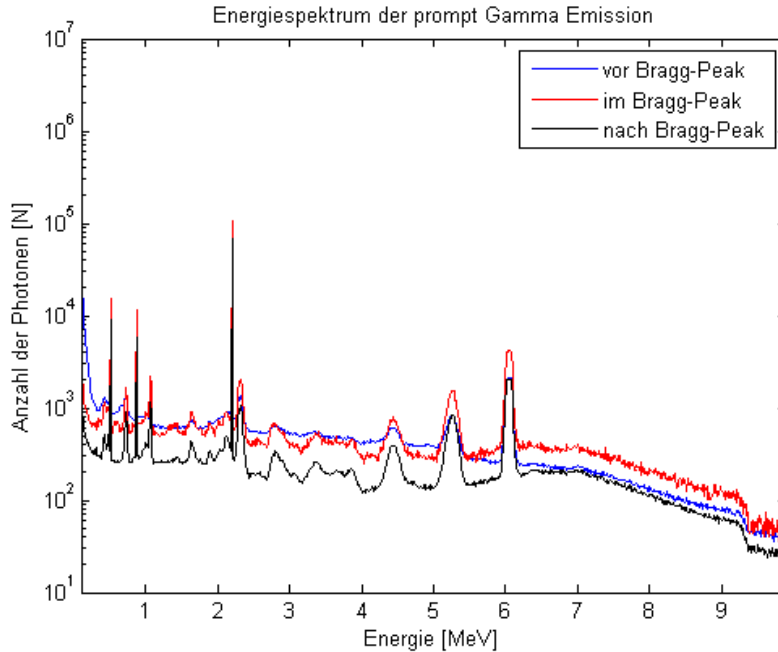
Figure 5.22: The energy spectra of produced gamma rays during an irradiation of a water phantom with 220 MeV/u carbon ions. Blue line maps the energy spectrum before the Bragg peak, the red line at the Bragg peak and the black line after the Bragg peak [6]
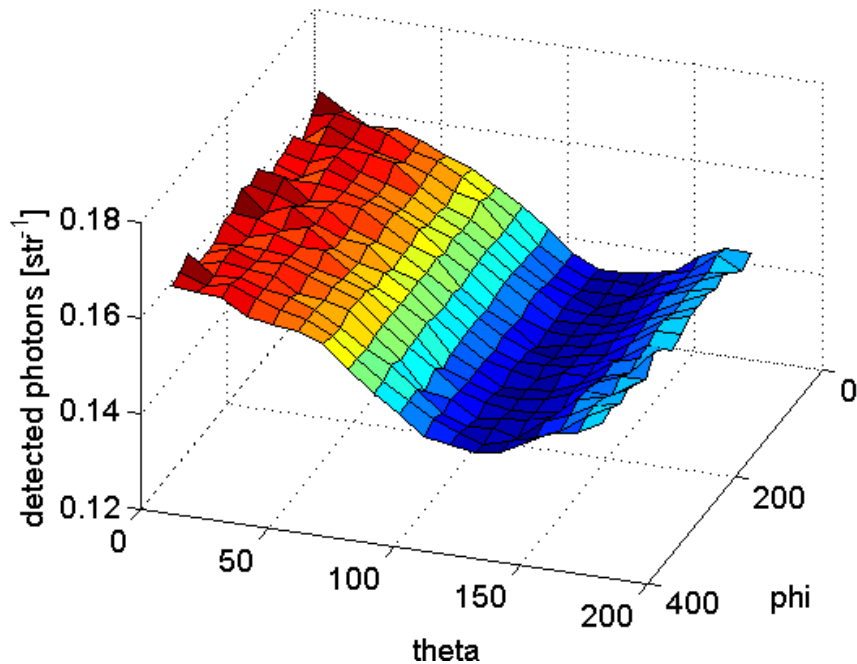
outside of the target.

Nonetheless the results show a correlation between the Bragg peak and a parameter of the produced photons, namely the simple production rate, whereas the functions of the energy spectra as shown in the figure 5.22 on page 44 remain nearly the same for the different measurement positions [6].

Additional to the measurements above the simulations were used for further investigations. The initiation for this were the results of GATE simulations which are discussed in a diploma thesis by Andreas Pichler [3]. These simulations treated the angular distribution of detected gamma rays outside of a water target irradiated by a carbon ion beam. Although it was used a specific geometry to diminish the influence of the shape of the water target on the measured angular distribution by using a spherical target whereby the calculated Bragg peak was right into the centre(cf. 5.23 on page 45), especially for higher primary carbon ion energies the results were unexpected. Figure 5.24 on page 46 shows the angular distribution for a 3400 MeV carbon ion beam. As expected an isotropic photon detection in ϕ direction can be seen, but the counts of detected photons sinks with a higher angle θ. Since in these simulations a value of $\theta = 180$ means a detection in the
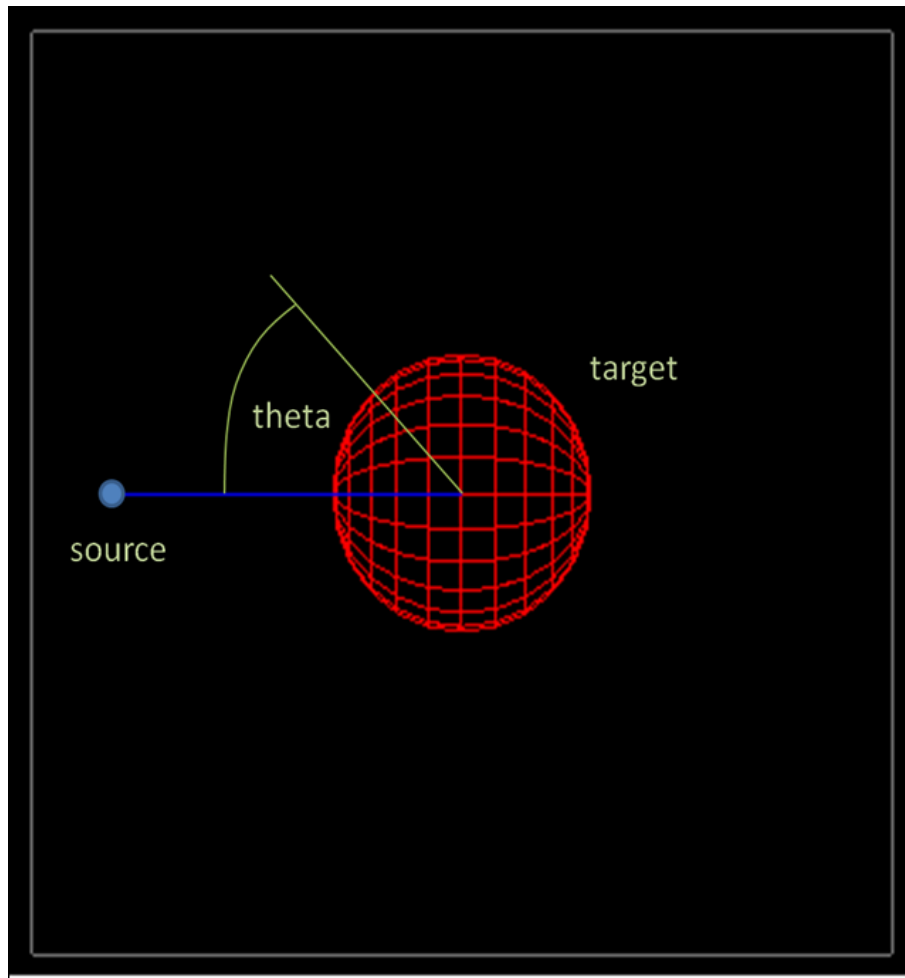
**Figure 5.23:** Geometry of the setup for measuring the angular distribution of prompt photons. [3]

Figure 5.24: Angular distribution of prompt photons for carbon ions hitting a water target at 285 MeV/u measured outside of the irradiated target. [3]

beam direction more photons are counted in the backward direction. A more exact analysis of a simulation executed with a primary energy of 2800MeV regarding the energy spectrum of the detected photons resulted in the graphs shown in figure 5.25 and 5.26 from page 47 on. As can be seen only for photons with an energy below 0.5 MeV the θ angle distribution differs from the intuitively expected measurement.

To prove and examine these results on base of the photon production directly in the irradiated target, the simulations with the geometry explained at the beginning of this section were used. Against the backdrop of computing time and resources additional to the described actor which provided the results presented above another group of actors were activated and attached in these simulations. Listing 5.7 on page 48 contains the used *Production And Stopping Actor* to measure the photon production in beam direction. In addition to the actor used for the total photon production an *angleFilter* was activated. As can be seen if the code of the actor is compared with the code for the used source (cf. 5.5 on page 41), this filter restricted the measured photons to those which are produced in beam direction or a cone of 45 degree in beam direction. With only small adaptations also actors for the other direction of the coordinate systems were included, as well as for the opposite directions.
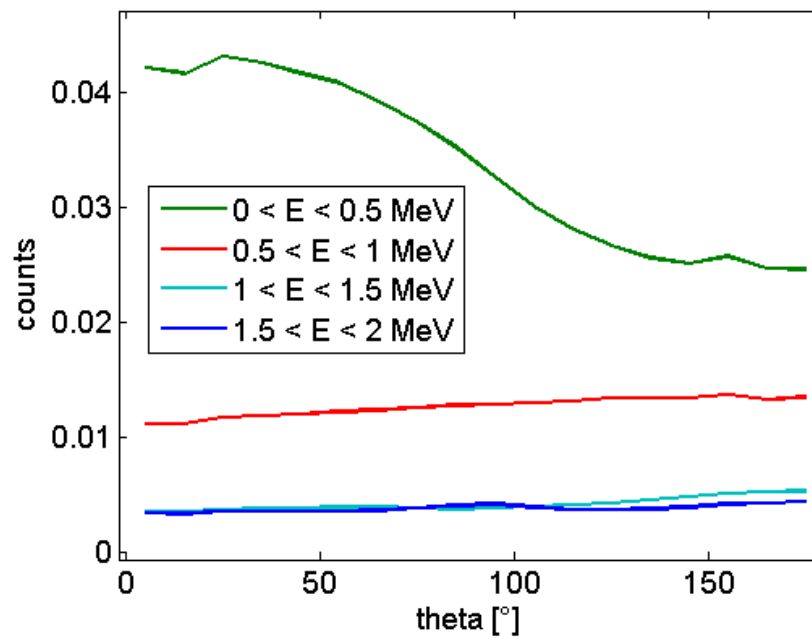
Figure 5.25: Angular distribution of different low photon energy ranges for carbon ions impinging on a water target at 240 MeV/u. [3]
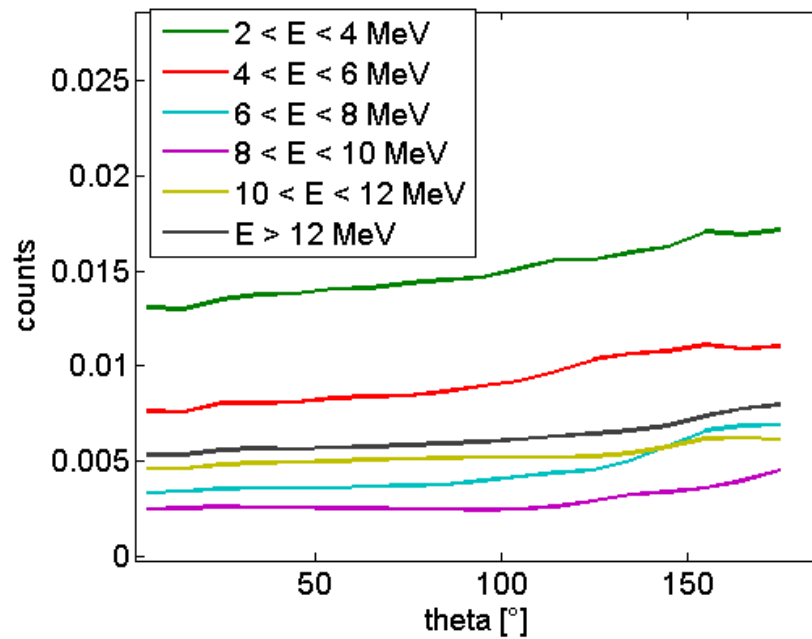

Figure 5.26: Angular distribution of different high photon energy ranges for carbon ions impinging on a water target at 240 MeV/u [3]

Listing 5.7: Example for the Production And Stopping Actor used for investigations on the produced photons in a specific direction during an radiotherapy

```
/gate/actor/addActor ProductionAndStoppingActor  Gamma_z+
/gate/actor/Gamma_z+/save
         Output/Primaerenergie_{primaerenergie}/Gamma_z+.txt
/gate/actor/Gamma_z+/attachTo      Phantom
/gate/actor/Gamma_z+/setResolution 1 1 1000
/gate/actor/Gamma_z+/stepHitType   post
/gate/actor/Gamma_z+/addFilter particleFilter
/gate/actor/Gamma_z+/particleFilter/addParticle gamma
/gate/actor/Gamma_z+/addFilter angleFilter
/gate/actor/Gamma_z+/angleFilter/setAngle 45
/gate/actor/Gamma_z+/angleFilter/setDirection 0 0 1
```

So altogether with the first actor which measured all photons seven actors were attached to the water target.

The following figures 5.27 and 5.28 from page 49 on show the complete results for those simulations. The first plot contains the results for a simulation with 2880 MeV carbon ions. The blue plotted function is already known from figure 5.21 since it shows the total photon production as a function of the penetration depth of the carbon ions. The Bragg peak is again marked by the vertical blue line. Furthermore the figure contains separate graphs for the photon production for each coordinate system direction. As noticeable the functions for the directions normal to the primary beam direction, namely the x+, x-, y+, y- graph in the figure, are one above the other. So in accordance to the results shown in figure 5.24 the angle distribution of the produced photons is isotropic in the angle ϕ. However the beam direction z+ and the opposite direction z- show deviant behaviour. Before the Bragg peak the count rate of produced photons in beam direction is significant higher than the one in the opposite direction. Also the results plotted in the other figure 5.28 support this behaviour. In contrast to the investigation on the angle distribution of the detected photons outside of the irradiated target the angle distribution of the produced photons remains as intuitive expected. Very well recognizable is that at and after the Bragg peak the distribution is getting quite isotropic. So it is not possible and not necessary to determine a position for a detector to measure preferred the photons produced in the Bragg peak.
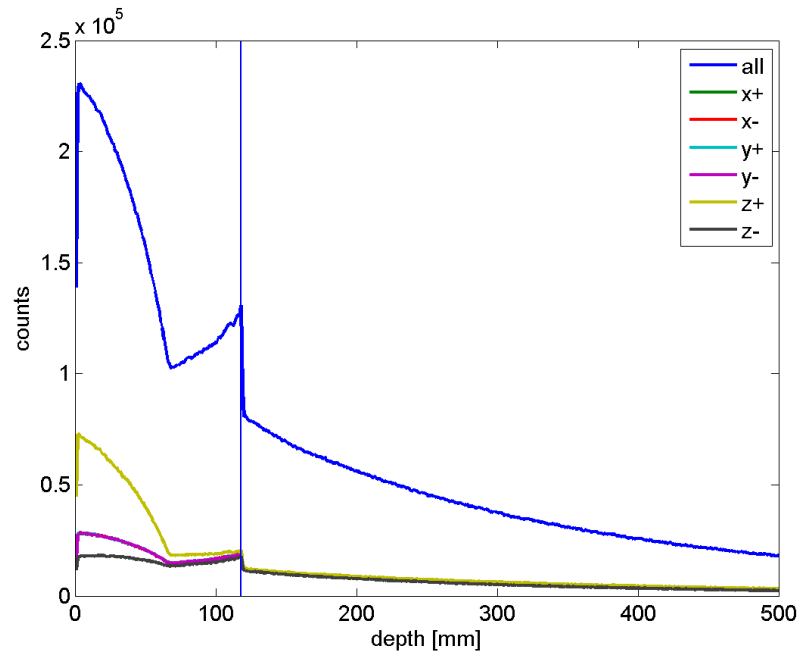
Figure 5.27: Angle dependent photon production for carbon ions impinging on a water target at 240 MeV/u
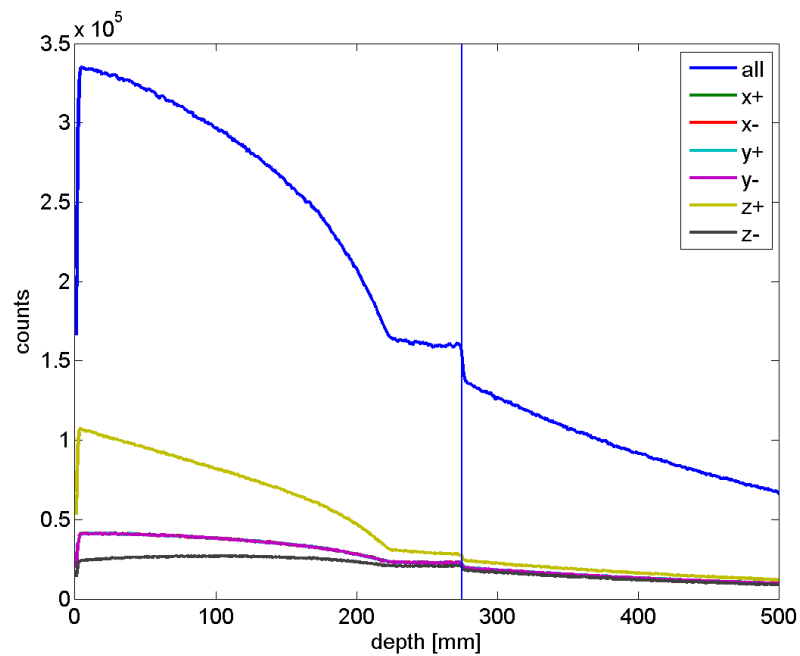
Figure 5.28: Angle dependent photon production for carbon ions impinging on a water target at 400 MeV/u

5.2.2 Energy resolution of the photon production

The former section 5.2.1 gave a fist simple impression of the photon production in an irradiated material and enabled to start more precise investigations. Since this general investigations could not avoid discrepancies referring to the results of other studies, these studies were a good starting point for the next simulations. As can be seen in figure 5.25 on page 47 there is a significant distinction between the plotted functions for different energy ranges in the measurement of the angular distribution. In consequence of this the simulations introduced in this section examined the photon production for different energy ranges of the produced photons.

The first step was again to build up the simulation setup. Actually there were only a few necessary adaptations to the simulation setup presented in section 5.2.1. The whole geometry including the source and the area to attach the actors on remained the same. The modifications referred only to the used actors. Instead of measuring the whole photon production at once, there were now several *Production And Stopping Actor* to divide the production in different energy ranges. To enable this another filter was used in addition to the already presented filters which restrict the measurement to the specific energy range. Listing 5.8 contains the code for this energy filter.

Listing 5.8: Example code to activate the the energy filter used in Gate for different actors

```
/gate/actor/{actore name}/energyFilter/setEmin  {emin}  MeV
/gate/actor/{actore name}/energyFilter/setEmax  {emax}  MeV
```

Instead of {actore name} the used id for the actual actor in the simulations has to be used and the entries {emin} and {emax} has to be replaced by the desired boundaries. Listing 5.9 shows one example of a used actor to measure the produced photons in an energy range of 2.5 to 2.6 MeV in beam direction.

Listing 5.9: Example code for a used *Production And Stopping Actor* for a specific energy range in forward direction

```
/gate/actor/addActor ProductionAndStoppingActor
                Gamma_E_2.5_2.6_z+
/gate/actor/Gamma_E_2.5_2.6_z+/save
      Output/Primaerenergie_{primaerenergie}
     /Gamma_E_{emin}_{emax}_z+.txt
/gate/actor/Gamma_E_2.5_2.6_z+/attachTo      Phantom
/gate/actor/Gamma_E_2.5_2.6_z+/setResolution 1 1 1000
```

```
/gate/actor/Gamma_E_2.5_2.6_z+/stepHitType    post
/gate/actor/Gamma_E_2.5_2.6_z+/addFilter particleFilter
/gate/actor/Gamma_E_2.5_2.6_z+/particleFilter/addParticle
                                             gamma
/gate/actor/Gamma_E_2.5_2.6_z+/addFilter angleFilter
/gate/actor/Gamma_E_2.5_2.6_z+/angleFilter/setAngle 45
/gate/actor/Gamma_E_2.5_2.6_z+/angleFilter/setDirection 0 0 1
/gate/actor/Gamma_E_2.5_2.6_z+/addFilter energyFilter
/gate/actor/Gamma_E_2.5_2.6_z+/energyFilter/setEmin  2.5  MeV
/gate/actor/Gamma_E_2.5_2.6_z+/energyFilter/setEmax  2.6  MeV
```

So as distinct from the section above not only one package composed of 7 actors were attached. One of such a package this time measured the energy depending photon production in all of the presented direction and the complete production. And such packages were used to measure the production in 0.1 MeV steps in therms of the energy, so the collected data contain an complete energy grid from 0 to 12 MeV photons.

Again to save computing time simultaneously also actor packages to measure the photon production for the most prominent peaks of the photon energy spectra (cf. figure 5.6 on page 27) and the energy ranges between them were attached. Cause of the amount of used actors and the linked amount of collected data the computing time increased significant, but nevertheless was a lot less then starting a own simulation for every actor package.

Tabular 5.3 on page 52 shows the energy ranges which were used to investigate on the behaviour of the prominent peaks. A closer consideration indicates some differences to the peaks of the former used energy spectra. The reason for this was the difference of the used Gate version. While the energy spectrum in figure 5.6 was measured with Gate version 6.1 the shown energy ranges for the prominent peaks in the listing are slightly shifted because of newer results by a newer Gate version 6.2. However the differences were quit weak, only the peak at about 6 MeV had a real reposition, but had no influence on our results as will be treated later on.

So the first evaluation of the collected data concentrated on the energy ranges used in the simulations shown in figure 5.25. To match the results the produced photons with an energy between 0 and 2 MeV were divided at 0.5 MeV into two separate energy ranges. Figure 5.29 on page 52 displays the production of 0.5 to 2 MeV photons as a function of the penetration depth. As ever the primary particles were 10^7 carbon ions which irradiated a water target. As expected the production of photons is higher in the forward direction then backwards and this behaviour remain the same for all other tested primary energies. Representatively figure 5.30 on page 53 contains the results for a primary energy of 4800 MeV.

The more interesting energy range of 0 to 0.5 MeV for the produced photons is shown

lower boundary	higher boundary
0.505 MeV	0.52 MeV
0.685 MeV	0.745 MeV
0.85 MeV	0.89 MeV
2.19 MeV	2.21 MeV
2.26 MeV	2.34 MeV
3.63 MeV	3.73 MeV
3.81 MeV	3.88 MeV
4.39 MeV	4.49 MeV
4.51 MeV	4.59 MeV
5.21 MeV	5.35 MeV
9.91 MeV	10.45 MeV

Table 5.3: Energy boundaries for the photons of the prominent peaks of the energy spectra of prompt gamma radiation obtained by simulations with Gate 6.2. These energy ranges were used to investigate on the photon production during radiotherapy
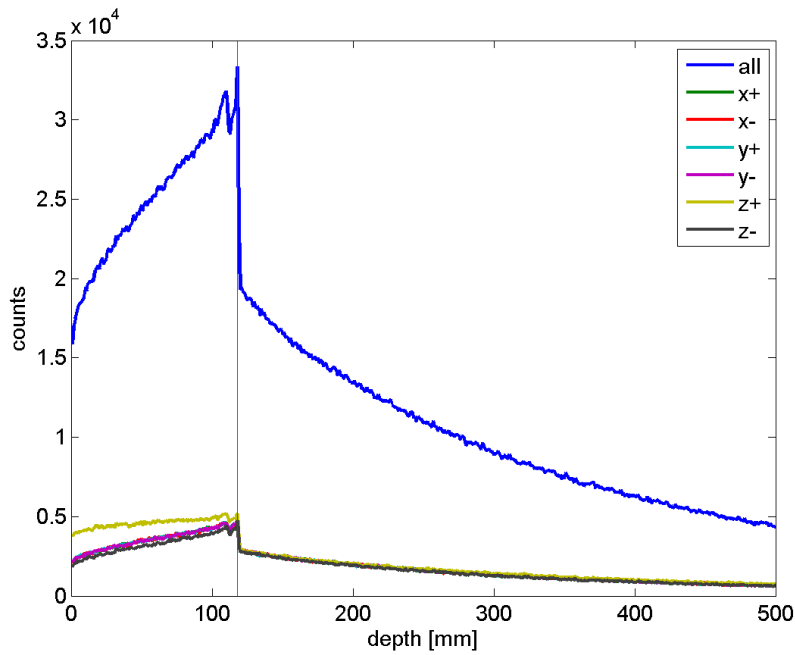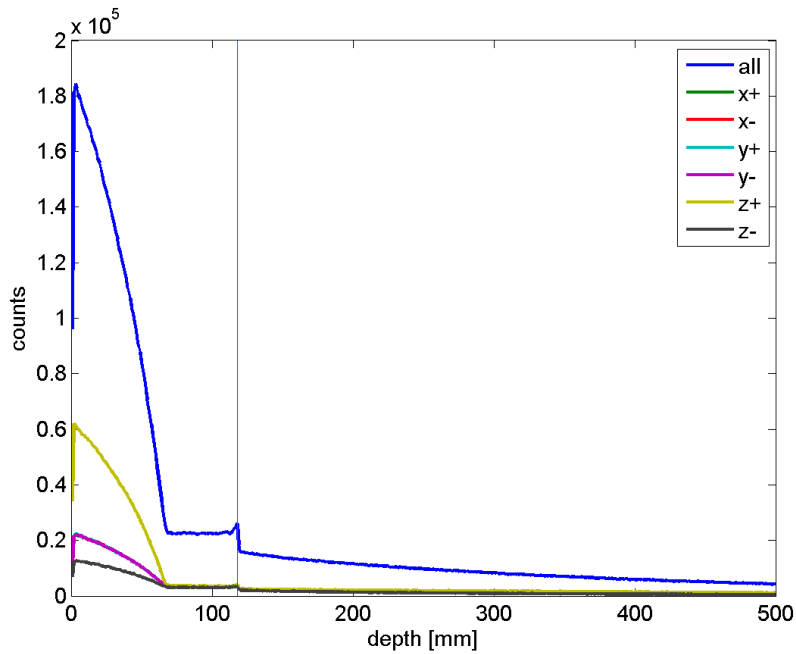

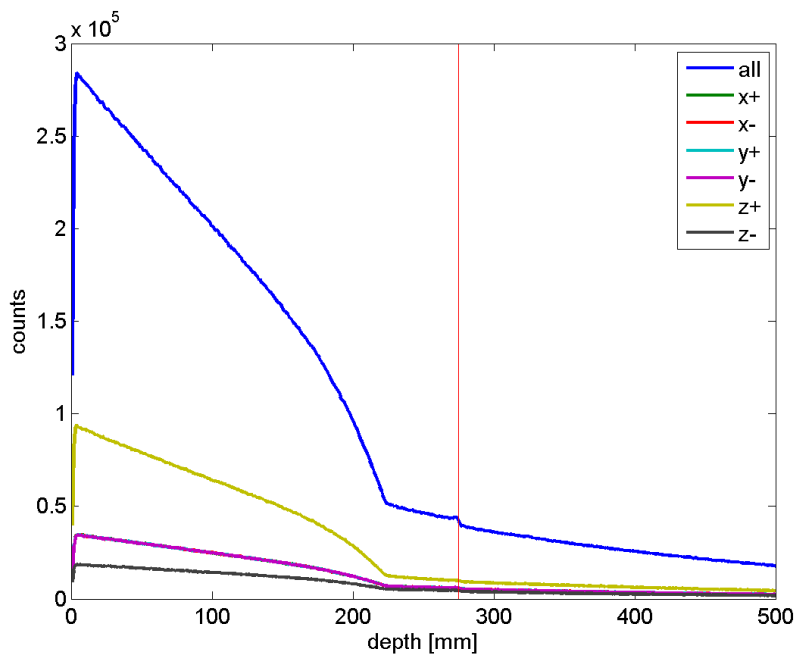**Figure 5.29:** 0.5 to 2 MeV photon production for 10^7 240 MeV/u carbon ions in a water target.
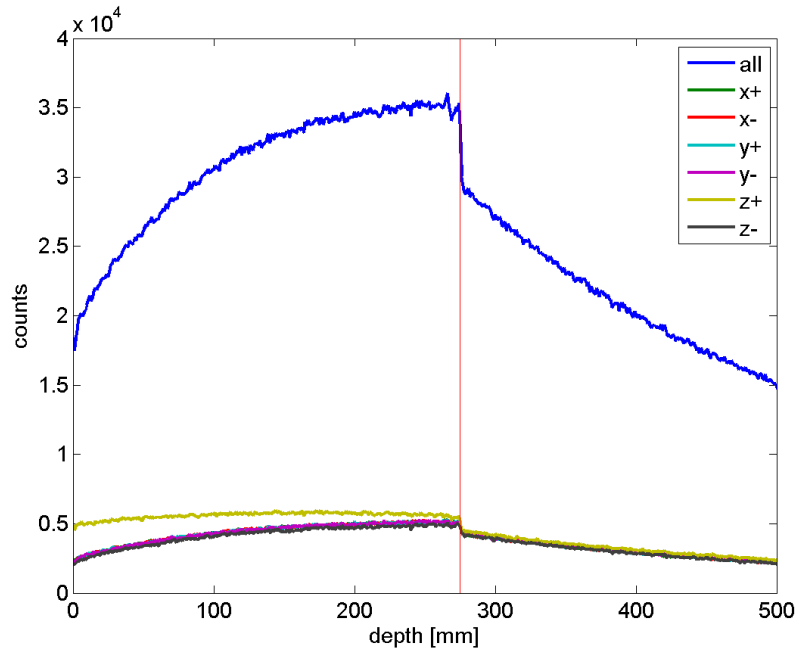
Figure 5.30: 0.5 to 2 MeV photon production for 10^7 400 MeV/u carbon ions in a water target.

in figure 5.31 and 5.32 from page 54 on. But also this graphics support the expected results of a preferred photon production in the forward direction of the primary carbon ion beam. However it can be seen that a majority of this low energy photons is produced in the target right from the beginning and the production rate fell off before the Bragg peak. Comparison of the figures is even an evidence for the independence of this effect from the chosen primary energy. So the reason for the counter intuitive effect in the results of the angle distribution of the detected photons outside of an irradiated material was not the direction the photons are produced, but a combination of the production depth and the attenuation of photons passing through the target. The photons with an energy below 0.5 MeV were produced mostly before the Bragg peak and at the same time these photons had the highest absorption rate of the checked photon energies. The photons produced in the forward direction had to pass a much longer way through the target and were absorbed much more before they got detected compared to the photons produced in the backward direction.

Another important result of these simulations could be recognized by a comparison of different photon productions for the same primary energy. The displayed data in figure 5.31 and 5.29 suggest that different energy ranges of the produced photons result in at least slightly different functions of the photon production. The signal of the Bragg
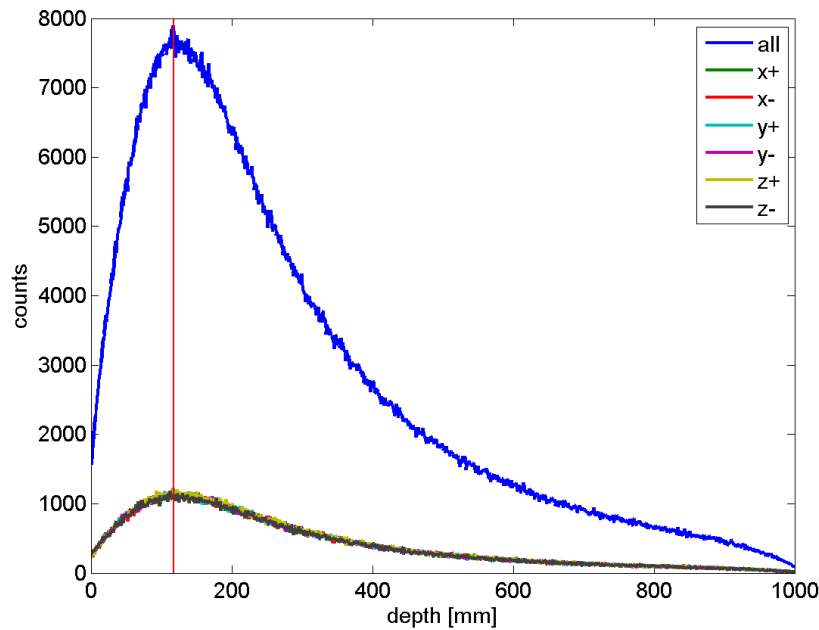
Figure 5.31: 0 to 0.5 MeV photon production for 10^7 240 MeV/u carbon ions in a water target.

Figure 5.32: 0 to 0.5 MeV photon production for 10^7 400 MeV/u carbon ions in a water target.

Figure 5.33: Production function of photons around 2.2 MeV for 10^7 240 MeV/u carbon ions and a water target

peak seems more significant for the photons above 0.5 MeV. Although the absolute value of the decrease of counted photons at the Bragg peak is nearly the same in both functions, the relative value differed a lot more if someone take into account the amount of photons produced before the Bragg peak for photon energies below 0.5 MeV. While the Bragg peak is still marked by a clear recognizable leap in the production function, the photons produced before the Bragg peak will reduce the significance during a measurement outside of the irradiated target for reasons of scattering and simply by their amount.

The results of the paragraph above suggest that it is possible to improve the significance of the Bragg peak by limiting the range of observed photons for an energy range with a preferably high significance and a sufficient high count rate. For this reason the collected data of the explained simulation at the beginning of this section for the most prominent peaks of the energy spectra as well as the ranges between them were analysed.

The first ground broke the peak of 2.2 MeV Photons in the photon production, because as recognizable in figure 5.6 on 27 these photons had the highest production rate and therefore may the highest influence. Like the known system figure 5.33 contains the graphical results for this most prominent peak for a primary energy of 2880 MeV for the carbon ions. First the results show that the photon production for this energy range is

completely isotropic instead of having a slightly preference in forward direction. This would be a good property for later measurements outside of the target course the detector placement is less strict. Second the production function for this energy range and a primary energy of 2880 MeV seems to have a good behaviour for the purpose of detecting the Bragg peak. As the red vertical line marks, the function has its maximum value at the Bragg peak and even if its not a sharp peak, it seems to be better then the functions of the photon production introduced yet. But if figure 5.33 is compared to the figures 5.34 on page 57 , which shows the same production function for different primary energies the problem would appear. On the one side the production function for a primary energy of 1440 MeV at least still have a slight peak at the marked Bragg peak, however the maximum of the function is not at the Bragg peak but after. On the other side for higher primary energies like 4800 MeV the peak nearly disappears completely and the maximum is shifted to the left what means before the Bragg peak. Because the reason for the 2.2 MeV Peak in the energy spectrum is the neutron capture of the hydrogen atoms [6] the production may is linked to the neutron production but for obvious reasons is not helpful for the investigations in this thesis.

Representative for most of the other prominent peaks figure 5.35 on page 58 shows the data for photons of about 4.55 MeV for a primary energy of 2880 MeV In difference to the 2.2 MeV Peak there is again a slight preference of the production in forward direction but it is not powerful enough to have any important influence. The maximum of the function is again at the Bragg peak which is marked by the red vertical line and shows this time a much more significant behaviour, namely a strong decrease right after the Bragg peak. Again compared with the results for 1440 and 4800 MeV carbon ions the energy range remain useful for the detection of the Bragg peak, although the peak also loses characteristic for higher energies. As figure 5.36 on page 59 shows the function of the resulting photon production for 1440 MeV primary energy has a very significant peak structure, and in contrast to the 2.2 MeV photons, the maximum remains at the position of the Bragg peak. Also for higher energies like 4800 MeV the function shows a decrease at the Bragg peak, and remain useful although the behaviour is getting less significant. What this all amounts to is that the behaviour of the most prominent 2.2 MeV photons is may an exception but also the investigations on the rest of the prominent peaks of the energy spectrum are not completely satisfying as the example for 4.55 photons shows.

As a consequence of this the photons with energies between the spectrum peaks were considered. Again the data of all these energy ranges were processed as the peaks before and they all showed quite similar results which are treated by using the example of the photons with an energy between 2.3 and 3.6 MeV. The functions in figure 5.37 on page
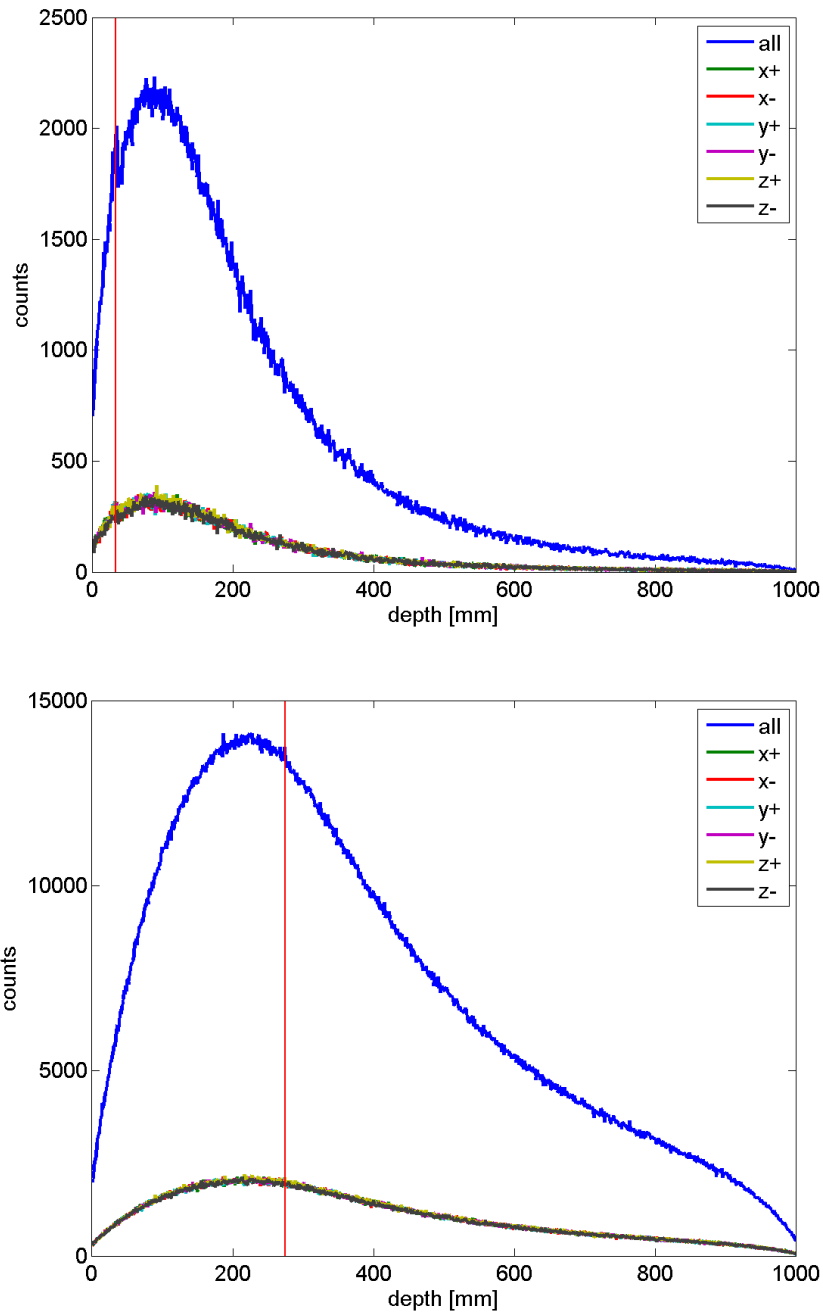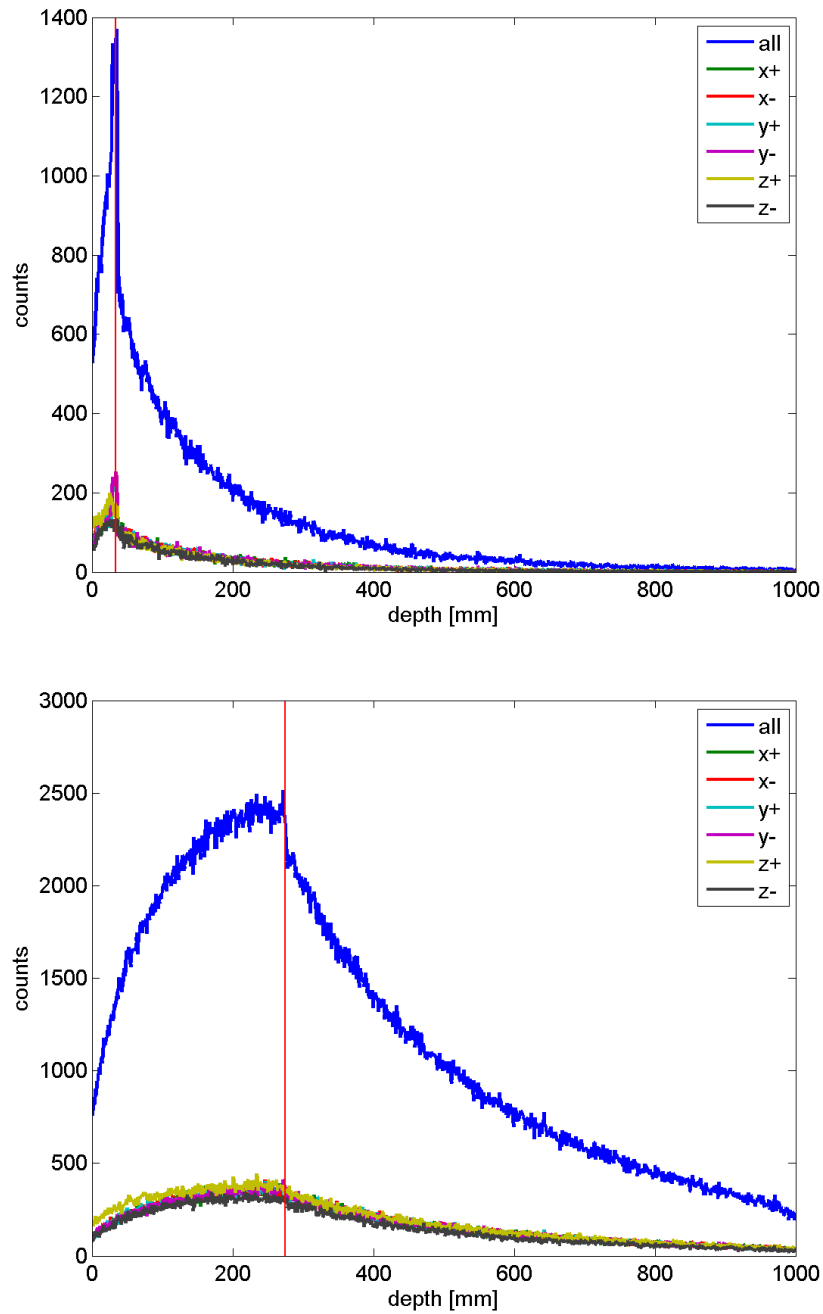
Figure 5.34: Production function of photons around 2.2 MeV for 10^7 carbon ions and a water target. The first function contains the results for a primary energy of 1440 MeV, the bottom one for 4800 MeV.
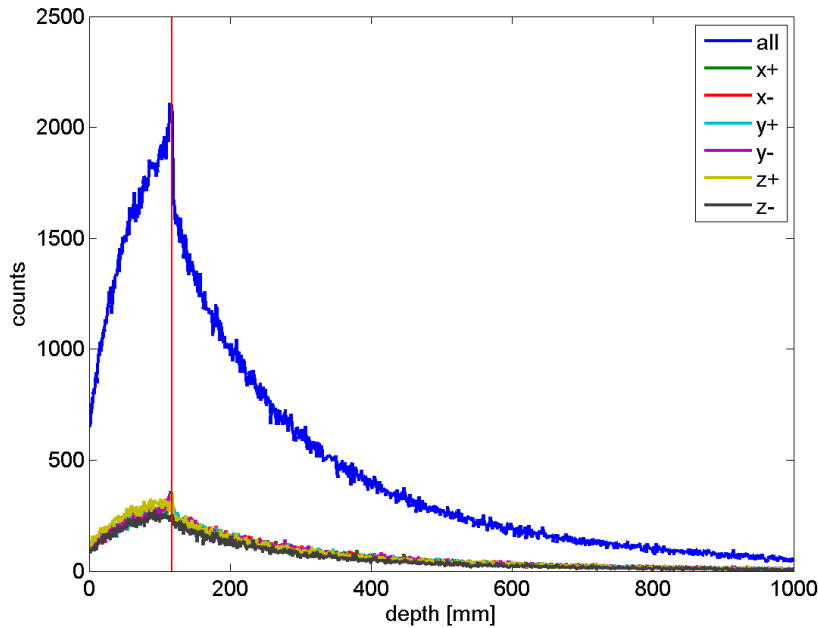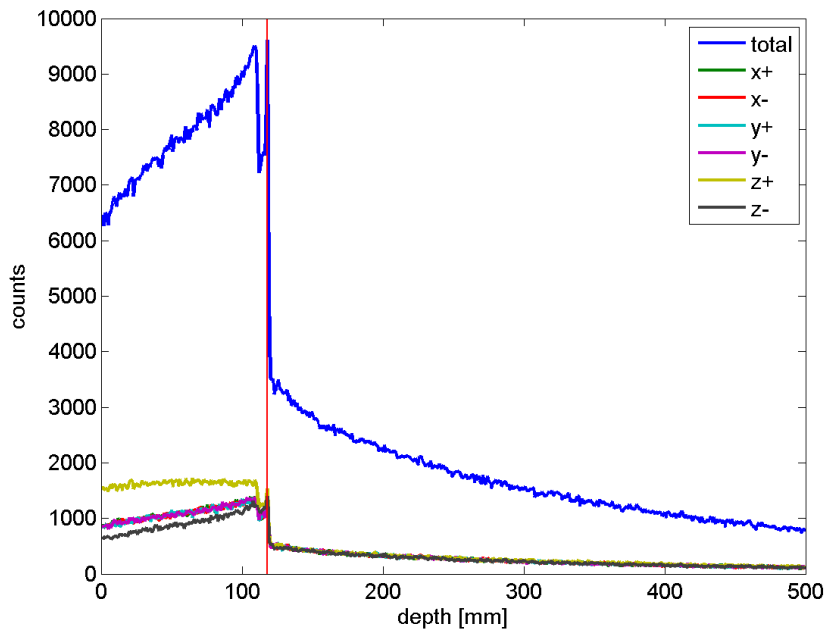
Figure 5.35: Production function of photons around 4.55 MeV for 10^7 240 MeV/u carbon ions hitting a water target.

60 are comparable to the function for the 4.5 MeV peak but the significance seems to be much higher. Although the resulting function has a decrease of produced photons slightly before the Bragg peak, the behaviour at the peak is still more significant than the behaviour of the former function. A compare of different primary energies is shown in figure 5.38 on page 60. The functions in this figure remain satisfying even for high primary energies.

All of the former discussed photon production functions with small energy boundaries may have a better significance than the total photon production, but the absolute counts of produced photons of course is relatively low. For this reason even the last introduced energy range for the produced photons supplies no satisfying results if the photons are measured outside of the irradiated target, because the scattering and especially the attenuation weak the significance [3]. To solve this problem the energy ranges has to be expanded again considering the informations gathered by the evaluation of the data of the single peaks and intermediate areas. For technical reasons in real measurements it is not practical to compose the photon production of different not connected energy ranges. To use the intermediate peak photons, the photons of the peaks have to be accepted. It is important to select a energy range with sufficient counts and at the same time sufficient significance. The previous investigations exclude only the photons below and inclusive
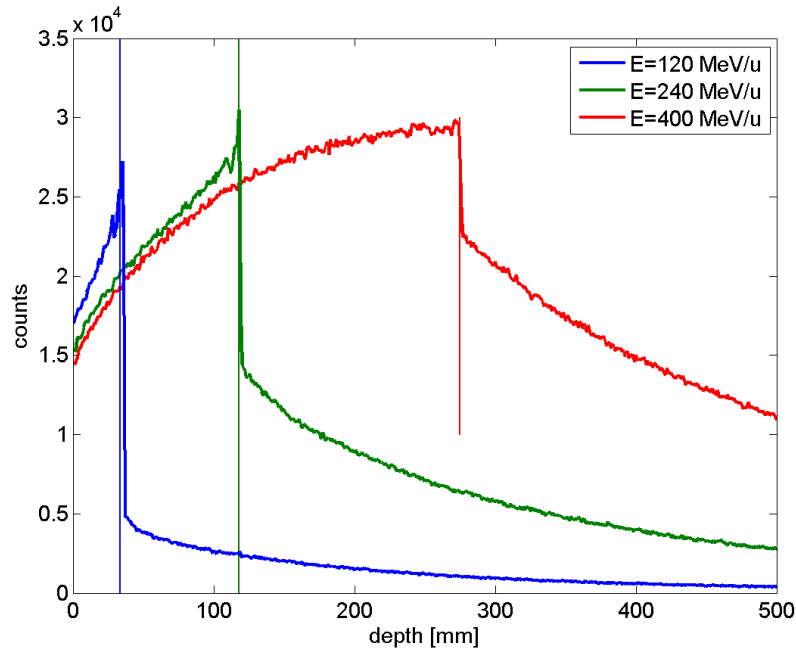
Figure 5.36: Production functions of 4.55 MeV photons for 10^7 carbon ions and a water target. At the top are the results for a primary energy of 1440 MeV, at the bottom for 4800 MeV.

Figure 5.37: Production function of 2.3 to 3.6 MeV photons for 10^7 240 MeV/u carbon ions irradiating a water target
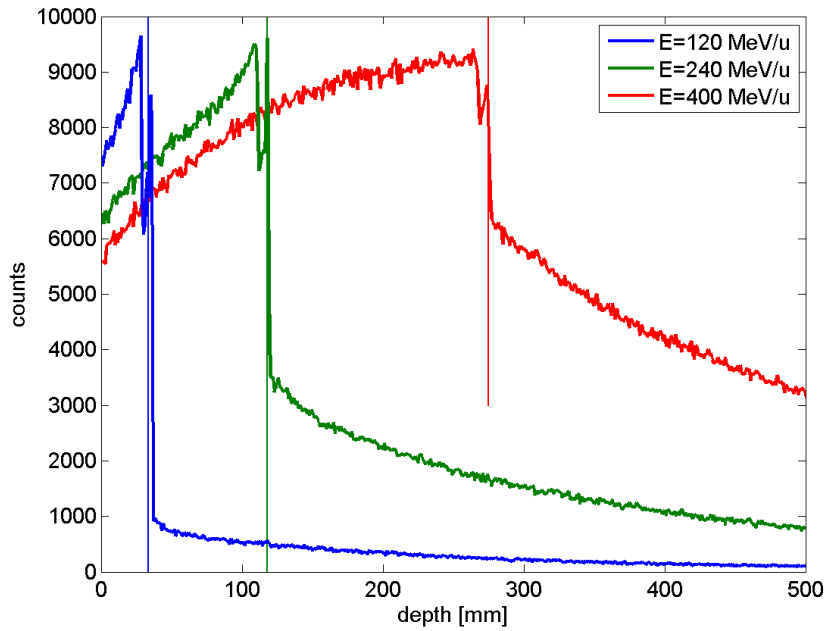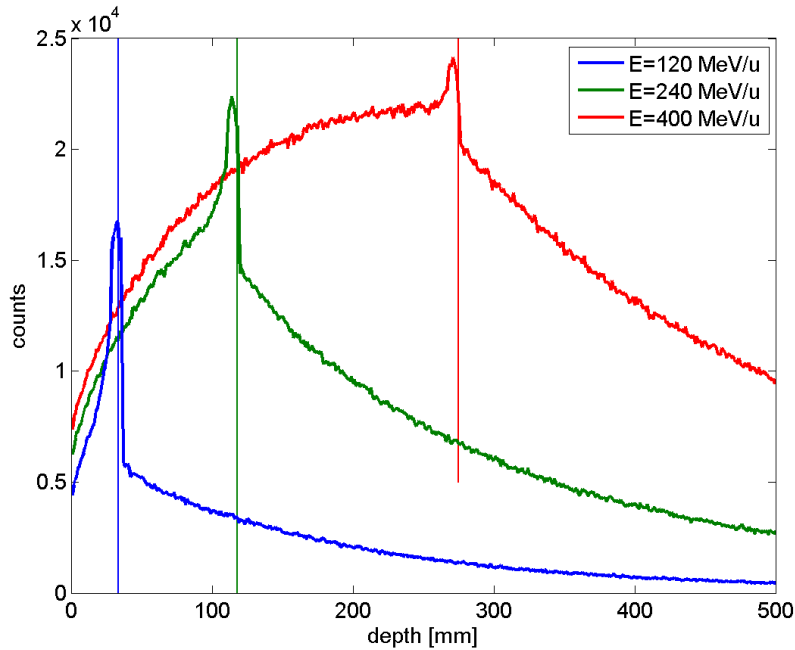

Figure 5.38: Comparison of the production function of 2.3 to 3.6 MeV photons for 10^7 carbon ions hitting a water target for different primary energies

Figure 5.39: Comparison of the production function of 2.3 to 6 MeV photons for 10^7 carbon ions hitting a water target for different primary energies. The function has a clear drop at the marked Bragg peak.

the 2.2 MeV peak, but although the higher peaks and energy ranges seen individually fulfil the requirements, they are not all compatible to each other. A close look at the energy spectra 5.22 on page 44 gives a first impression of the different behaviour of the photon production. A comparison of the three plotted functions for an energy below 6 MeV shows that the photon production has a drop after the Bragg peak cause the blue and red plotted function which represent the photon production before and at the Bragg peak are nearly in the same count range, while the black line, representing the photon production after the Bragg peak is much lower in view of the fact that a logarithmic plot is used in the figure. As opposed to this the photon production above 6 MeV changes. In this area the blue and the black line are next to each other but the red line representing the Bragg peak show much higher photon counts. So in this energy range the photon production has a real peak at the Bragg peak instead of a drop after the Bragg peak.

Figure 5.39 on page 61 shows the production function for the most promising energy boundaries between 2.3 and 6 MeV. If the plotted functions are compared to the former functions, it is recognize able, that the signal of the Bragg peak is on the one side more significant than the signal in figure 5.36 of the 4.55 MeV peak and on the other side, even if the signal is may not as significant as the signal in figure 5.38 at least the count rates

Figure 5.40: Comparison of the production function of 6 to 12 MeV photons for 10^7 carbon ions hitting a water target for different primary energies. The function has a clear peak at marked the Bragg peak.

are much higher.

The penetration dependent count rates of the production of 6 to 12 MeV photons is plotted in figure 5.40 on page 62 and shows the announced peak at the Bragg peak. The count rates are a few lower and the relative signal at the Bragg peak is not as significant as for the other energy range. Ultimately its necessary to investigate what form of signal and what energy ranges are more easy to handle in a real measurement.

Just for comparison figure 5.41 on page 63 contains the production functions for the photons between 2.3 and 12 MeV. Indeed the count rats of course are rising but the significance seems to be a bit lower then for the individual energy ranges.

5.2.3 Widening of the photon production

Up to that point all the simulations and the analysis only studied the photon production as a function of the penetration depth of the primary carbon ion beam. But to realize a recalculation of the photon production after measuring the produced photons outside of a irradiated target more informations will be needed. Especially if the photons are detected by a full tracking and the most likely origin is recalculated it is important to
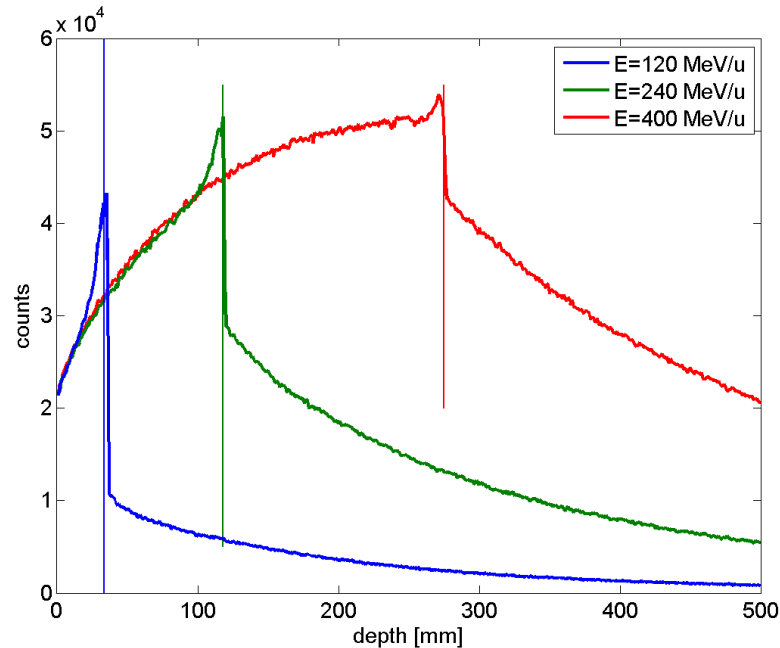
Figure 5.41: Comparison of the production function of 2.3 to 12 MeV photons for 10^7 carbon ions hitting a water target for different primary energies.

have not only information about the photon production as a function of the penetration depth but also as a function of the radial distance from the primary ion beam. For this reason a new simulation was built up. Most of the setup remain untouched in comparison to the former simulations so figure 5.20 on side 41 still gives a proper impression of the used geometry. Again a cylindrical water phantom with a radius of 30 centimetre and a high of 100 centimetre was used and the source produced a carbon ion beam which passes the target right through its axis. Based on informations provided by Herman Fuchs from the Department of Radiation Oncology of the medical university of Vienna the source was changed slightly to adjust it to realistic radiotherapies. The following code 5.10for the used source defines a different shape for the primary beam. Although the shape of the beam is still a circle, the border of the beam is not as unrealistic sharp as for former simulations. Instead a realistic Gaussian decrease was used.

Listing 5.10: GATE code of the used source for investigation on the widening of the photon production

```
/gate/source/addSource      C12        gps
/gate/source/C12/gps/particle          ion
/gate/source/C12/gps/ion               6 12 +6 0
```

```
/gate/source/C12/gps/energytype        Mono
/gate/source/C12/gps/monoenergy        2880 MeV
/gate/source/C12/gps/pos/type          Beam
/gate/source/C12/gps/pos/shape         Circle
/gate/source/C12/gps/pos/sigma_x 3 mm
/gate/source/C12/gps/pos/sigma_y 3 mm
/gate/source/C12/gps/pos/centre        0.0 0.0 -60.0 cm
/gate/source/C12/gps/direction         0 0 1
```

The precise idea of the simulation was to separate the photon production into two parts. The first part should be the photons which were produced inside of the primary carbon ion beam, and the second part should be the photons produced outside by secondary particles or already scattered carbon ions. In order to measure this widening of the photon production the used water phantom had to be adapted. Similar to the measurement devise in section 5.1 the water target was divided into two areas and the photon production was measured for each area individually as a function of the penetration depth. Listing 5.11 contains the additionally code for this kind of phantom.

Listing 5.11: Code of the divided phantom for investigation to the widening of the photon production

```
/gate/Phantom/daughters/name Innen
/gate/Phantom/daughters/insert cylinder
/gate/Innen/geometry/setRmin 0 mm
/gate/Innen/geometry/setRmax 6 mm
/gate/Innen/geometry/setHeight 100 cm
/gate/Innen/placement/setTranslation 0. 0. 0. m
/gate/Innen/setMaterial G4_WATER
/gate/Innen/vis/setColor blue
/gate/Innen/vis/forceWireframe

/gate/Phantom/daughters/name Aussen
/gate/Phantom/daughters/insert cylinder
/gate/Aussen/geometry/setRmin 6 mm
/gate/Aussen/geometry/setRmax 300 mm
/gate/Aussen/geometry/setHeight 100 cm
/gate/Aussen/placement/setTranslation 0. 0. 0. m
/gate/Aussen/setMaterial G4_WATER
/gate/Aussen/vis/setColor blue
```

```
/gate/Aussen/vis/forceWireframe
```

As noticeable the target cylinder was divided into an inner cylinder till 6 mm radius and an outer one for the rest. The reason for this parameters is the fact that for a Gaussian function 95% of the values are inside an area of 2 sigma. Regarding the fact that the carbon ion beam does not wide in a typical treatment depth and consider the used code for the carbon ion source which had a sigma value of 3 mm, it is apparent that all photons produced with less radial distance than 6 mm from the cylinder axis were within 2 sigma of the carbon ion beam.

Last but not least also the used actors were adapted. Instead of measuring the production in all direction individually, only the total photon production as a function of the penetration depth was measured, but sill the production was divided into small energy ranges of 100 keV. For this reason again all the already discussed energy ranges and prominent peaks could be analysed. Listing 5.12 shows the used code for the actors whose parameters are already known from former simulations.

Listing 5.12: Code of a reference actor for investigation on the widening of the photon production. The alias were replaced by the respective energy ranges

```
/gate/actor/addActor ProductionAndStoppingActor
                            Gamma_E_{emin}_{emax}_r_0
/gate/actor/Gamma_E_{emin}_{emax}_r_0/save
                Output/Production/{emin}_{emax}_r_0_Gamma.txt
/gate/actor/Gamma_E_{emin}_{emax}_r_0/attachTo      Innen
/gate/actor/Gamma_E_{emin}_{emax}_r_0/setResolution 1 1 1000
/gate/actor/Gamma_E_{emin}_{emax}_r_0/stepHitType   post
/gate/actor/Gamma_E_{emin}_{emax}_r_0/addFilter
                                            particleFilter
/gate/actor/Gamma_E_{emin}_{emax}_r_0/particleFilter/
                                addParticle    gamma
/gate/actor/Gamma_E_{emin}_{emax}_r_0/addFilter energyFilter
/gate/actor/Gamma_E_{emin}_{emax}_r_0/energyFilter/setEmin
                                            {emin}  MeV
/gate/actor/Gamma_E_{emin}_{emax}_r_0/energyFilter/setEmax
                                            {emax}  MeV


/gate/actor/addActor ProductionAndStoppingActor
                            Gamma_E_{emin}_{emax}_r_6
/gate/actor/Gamma_E_{emin}_{emax}_r_6/save
```
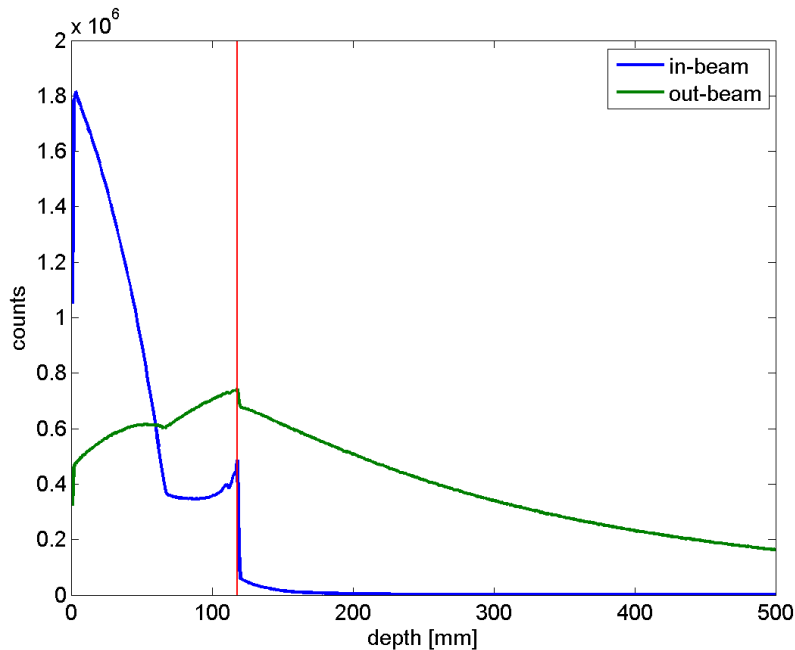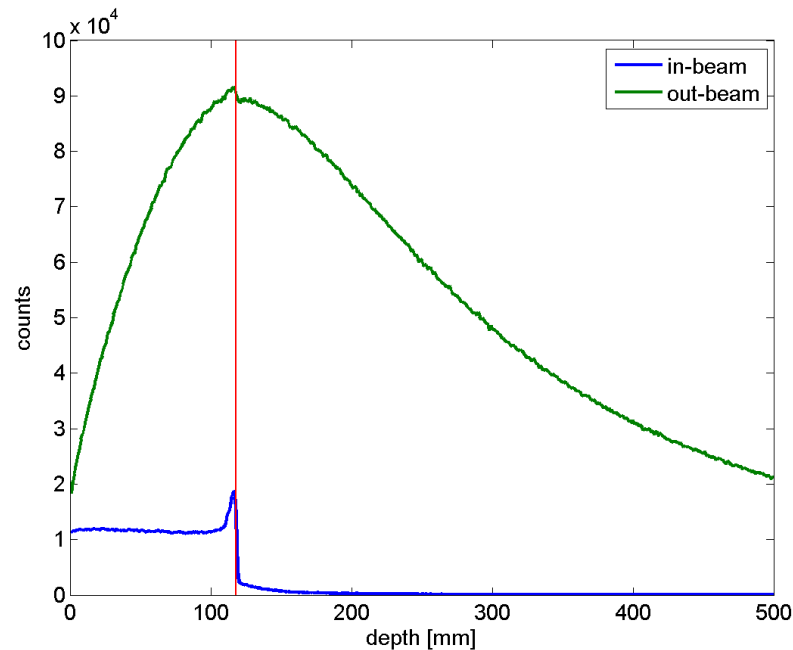
Figure 5.42: Comparison of the 'in beam' and 'out beam' production function of photons for 10^8 carbon ions hitting a water target with 2880 MeV.

```
                Output/Production/{emin}_{emax}_r_1_Gamma.txt
/gate/actor/Gamma_E_{emin}_{emax}_r_6/attachTo         Aussen
/gate/actor/Gamma_E_{emin}_{emax}_r_6/setResolution 1 1 1000
/gate/actor/Gamma_E_{emin}_{emax}_r_6/stepHitType      post
/gate/actor/Gamma_E_{emin}_{emax}_r_6/addFilter
                                          particleFilter
/gate/actor/Gamma_E_{emin}_{emax}_r_6/particleFilter/
                              addParticle        gamma
/gate/actor/Gamma_E_{emin}_{emax}_r_6/addFilter energyFilter
/gate/actor/Gamma_E_{emin}_{emax}_r_6/energyFilter/setEmin
                                          {emin}  MeV
/gate/actor/Gamma_E_{emin}_{emax}_r_6/energyFilter/setEmax
                                          {emax}  MeV
```

The fist data were processed for a medium primary energy of 2880 MeV for the used carbon ions and a number of 10^8 primary particles. Figure 5.42 on page 66 contains the analysis for the whole produced photons till an energy of 12 MeV. The functions show that the significance of the marked Bragg peak is extremely high also if all photon energies are used, as long as the analysis is focused on the photons produced directly by the primary

Figure 5.43: Comparison of the 'in beam' and 'out beam' production function of 2.1 to 2.3 MeV photons for 10^8 carbon ions hitting a water target with 2880 MeV.

carbon ion beam. Nevertheless as will be shown the significance could be raised again by using a favourable energy range.

As in the section 5.2.2 above also the most prominent peaks of the photon spectrum were analysed. Representative for all the peaks the following graphic 5.43 on page 67 includes the data of the 2.1 to 2.3 MeV photons for the medium primary energy of 2880 MeV. Although the included 2.2 peak has some strange behaviour as explained in the former section, the results of this simulations gives a good impression of the impact of the production point on the form of the production function. The green plotted production function of the photons produced outside of the primary carbon ion beam has a remarkable resemblance with the function shown in figure 5.33 on page 55 which contains the production function for the complete 2.2 MeV peak. But the blue painted function for the 'in beam' photons shows a high significance and a sharp drop right at the Bragg peak. If figure 5.44 on page 68 is taken into account, the effect of radial distance to the primary beam is even more impressive. This figure shows the results for a lower primary energy of 1440 MeV and as expected the plotted outer photon production has a shift which is not liked to the shift of the Bragg peak. But the inner photon production has again a very significant drop at the Bragg peak.
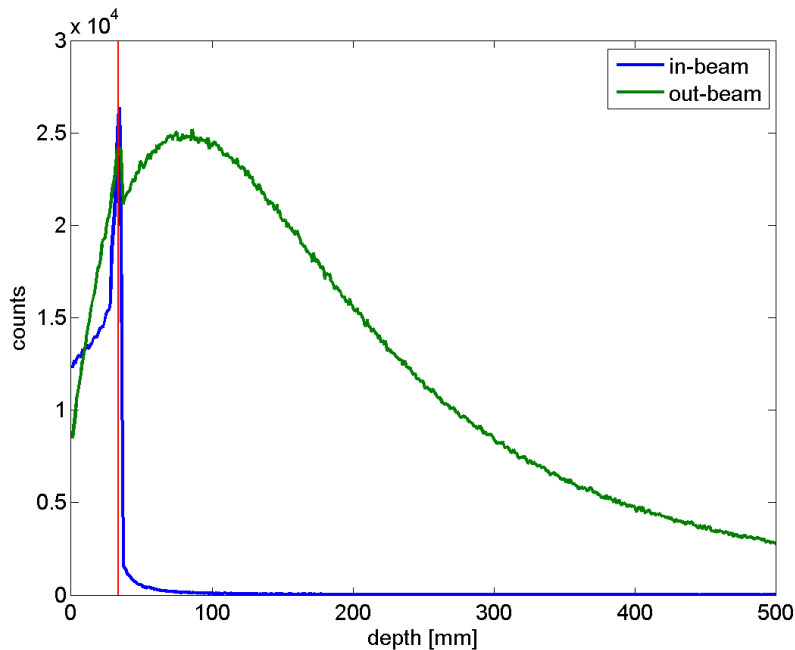
Figure 5.44: Comparison of the 'in beam' and 'out beam' production function of 2.1 to 2.3 MeV photons for 10^8 carbon ions hitting a water target with 1440 MeV.

So against the previous scepticism also the 2.2 MeV photons would be useful for the detection of the Bragg peak, but it would be necessary to differentiate the origins of the photons. This may be realized by a complete tracking of the detected photons or by a special geometry including collimators for example which filter the 'in beam' photons.

The other possibility is to search again for a energy region, where the outer produced photons have not that much influence. For that reason the collected data were used to compare the counts of in beam and out beam produced photons as a function of their energy. As figure 5.45 on page 69 shows the known most prominent peaks have a much higher influence on the energy spectrum of the photons produced outside of the primary ion beam. Since the previous investigations have shown that the energy regions containing a peak in the photon production are not as significant for the Bragg peak detection as the regions in between the assumption is suggested that the important parameter for the significance of the Bragg peak is the amount of photons produced inside the primary beam. In figure 5.45 it is recognizable that the photon production seems to be divided into two areas. In the first area, which are the photons below an energy of 6 MeV, the counts of in beam produced photons is quite high but unfortunately many of the prominent peaks disturb the signal. The area above 6 MeV contains not that many peaks, but if the logarithmic plot is considered the divergence of the in and out beam photons has an
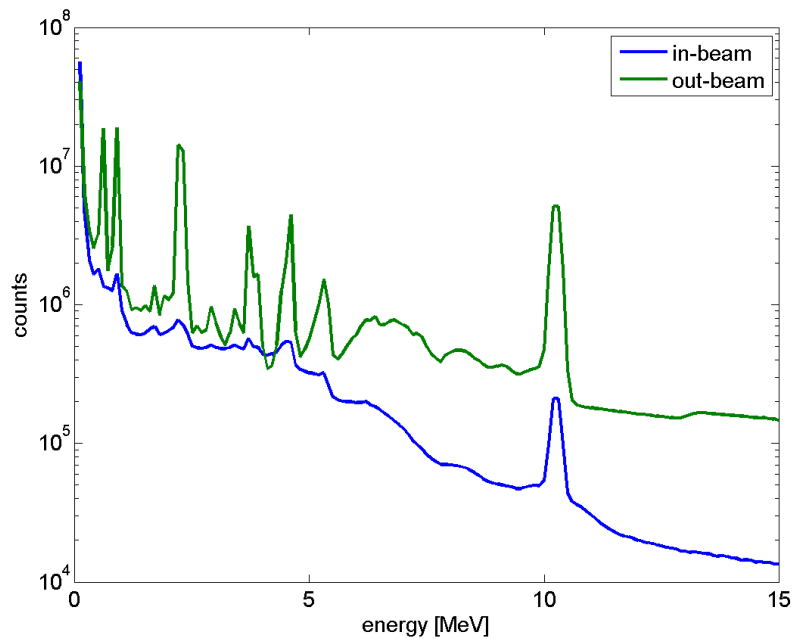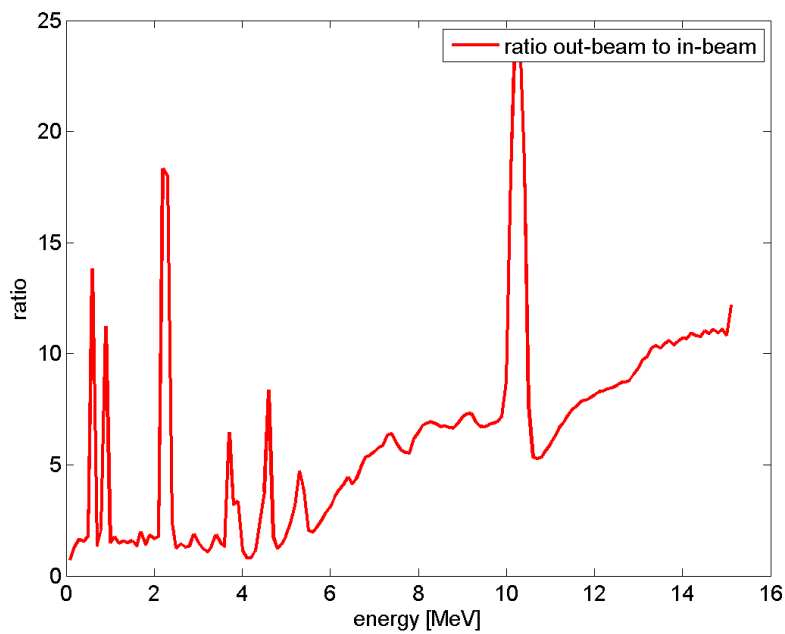
Figure 5.45: Comparison of the 'in beam' and 'out beam' photon production for 10^8 carbon ions hitting a water target with 2880 MeV.

adverse ratio also without peaks so the signal is also faded.

For a better overview figure 5.46 on page 70 shows the ratio of the 'out beam' production to the 'in beam' production. This means the lower the value of the ratio the less faded would be the signal of the inner photon production by the 'out beam' photons. On the one hand the plot explains clearly that the ratio is getting worse for energies above 6 MeV. On the other side we already know that the photons with energies under 2 MeV also don't have a very useful signal and as the plot shows the 2.2 MeV photons have a ratio witch is a way to high. If all this is brought together the result remains the same as in the section before. Also based on this ratio the best energy range of produced photons to get a high significance of the Bragg peak is the energy range between 2.3 and 6 MeV.

Figure 5.47 on page 70 finally contains the production function for photons between 2.3 and 6 MeV divided into the photons produced outside and inside of the primary carbon ion beam. As treated in section 5.2.2 the significance for this photons is quite high and independent of the primary energy. Nevertheless also these results point out that the significance can be improved extremely if the measurement device can distinguish between in and out beam photons.
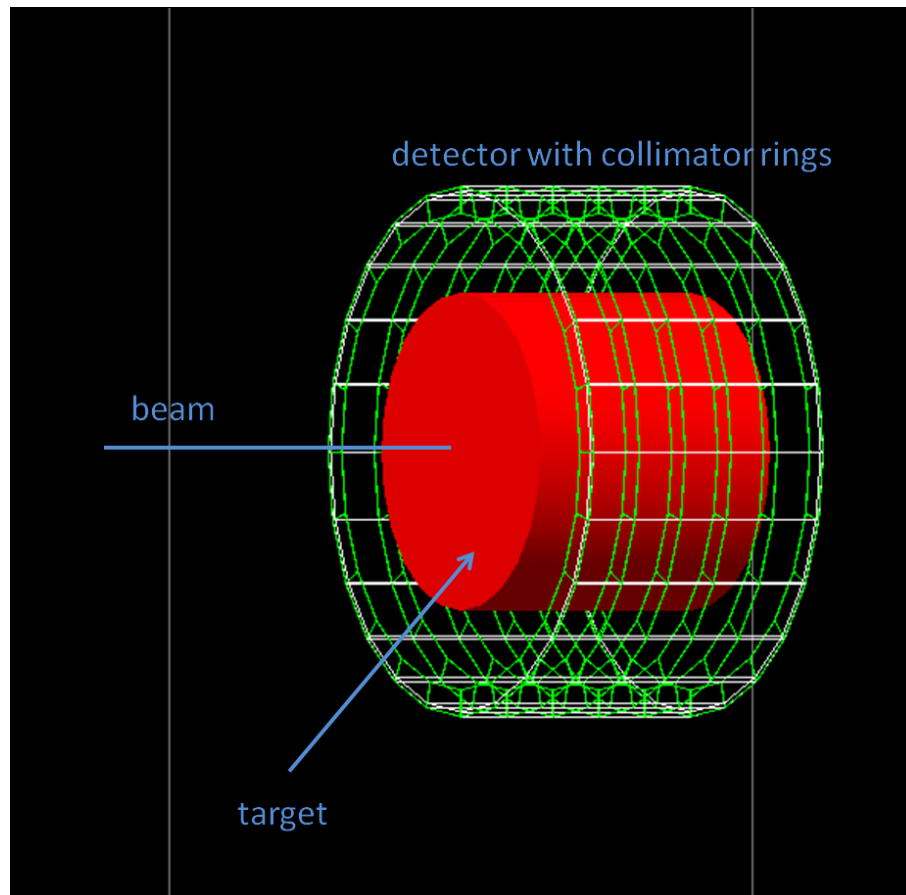
Figure 5.46: Ratio of the 'out beam' to the 'in beam' photon production for 2880 MeV carbon ions hitting a water target.
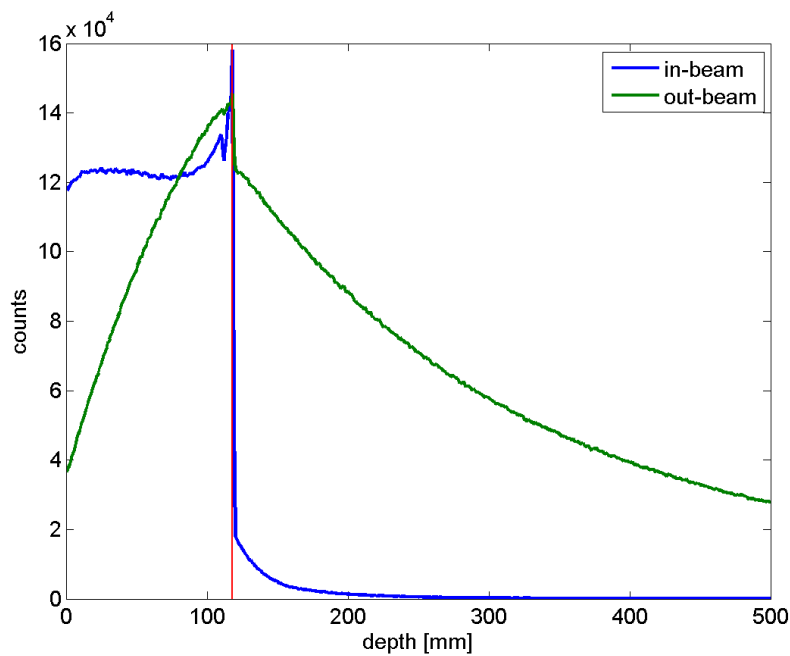
Figure 5.47: Comparison of the 'in beam' and 'out beam' production function of 2.3 to 6 MeV photons for 10^8 carbon ions hitting a water target with 2880 MeV.

Figure 5.48: Experimental setup for investigations on detected photons during an carbon ion therapy [3].

5.3 Photon detection

This section treats the transition from the photon production directly in the irradiated material to the photons detected with measurement devices outside of the target. In contrast to the sections above the following investigations don't focus on collecting new data, but use the gathered informations to find a correlation between the production function and detected photons.

### 5.3.1 Detector geometries employing an ideal collimator

The data used in this sections were collected by a simulation which was made as part of a master thesis [3]. At this point the setup of the simulation is only explained shortly. As figure 5.48 on page 71 shows the geometry remained nearly the same but as distinct from
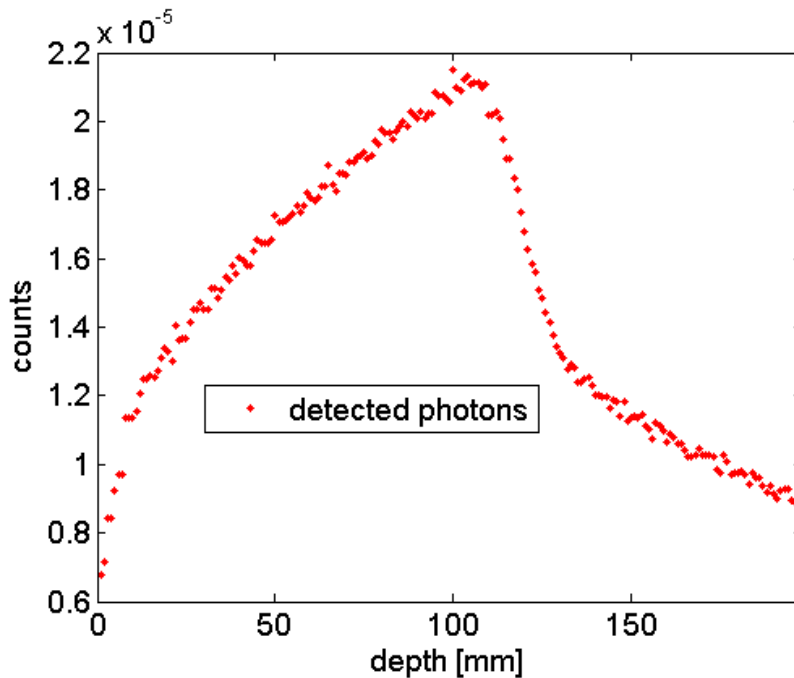
Figure 5.49: Detected photons in an energy range from 2.3 to 6 MeV for 2880 MeV carbon ions irradiating a water target as a function of their likely origin [3].

the investigations on the photon production the measurement device was built outside of the target. The detected photons were again measured as a function of the penetration depth of the primary carbon ion beam. To match the detected photons to their likely origins ideal collimators were used. This collimators should minimize the influence of photons which were not produced in the respective depth or were scattered so that their origin is not assignable. Although the results of section 5.2.3 propose techniques which distinguish 'in' and 'out' beam photons, this simulation only differentiated the depth of the photon origin. The source and target material remain the same as in the former sections.

Figure 5.49 on page 72 presents the data of this simulation in a graphical way. The plot shows the detected photons as a function of the penetration depth respectively of their likely production place. As distinct from the plots above the counts are not the absolute detected values but the detected counts per primary carbon ions. Nevertheless the behaviour remains the same, as the values were only rescaled by a factor. Although the figure shows the data for a energy range from 2.3 to 6 MeV of the photons which was the most promising energy range in the previous investigations, their is no drop as significant and as sharp as in the photon production of the same energy range shown in figure 5.50 on page 73
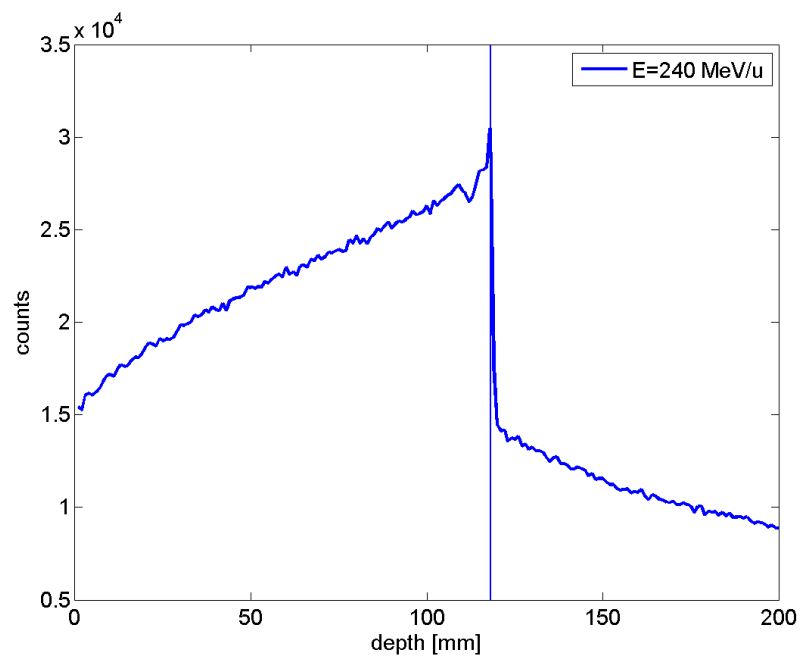
Figure 5.50: Simulated photon production in a energy range from 2.3 to 6 MeV for 2880 MeV carbon ions irradiating a water target as a function of the penetration depth.
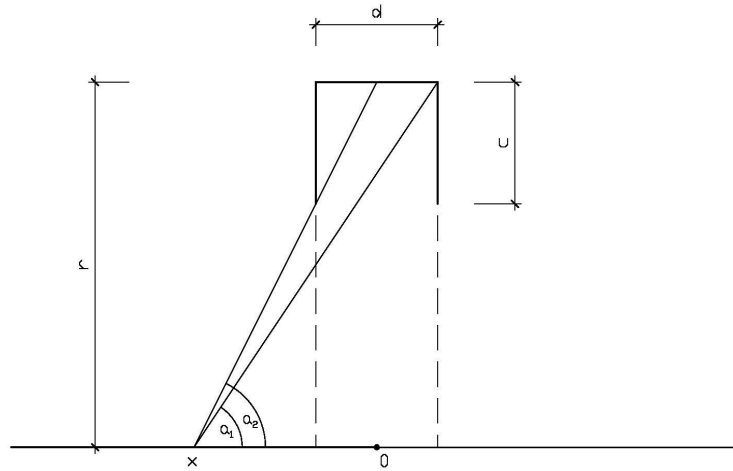
Figure 5.51: Abstract drawing of the experimental setup and the solid angel for a production spot and one detector cell.

To clarify the difference between these two figures it is necessary to look closer at the geometrical setup. Depending on the production place of a photon and its distance in beam direction from a specific detector part the probability to get detected was modified. Outline 5.51 on page 74 shows a plane abstract drawing of the geometry. On top is a detector cell with two collimators next to each side. Depending on the distance 'r' of the detector from the beam axis,the width 'd' of the detector, the length 'c' of the collimator and the distance 'x' of the production spot from the foot of the detector the probability of a photon to make its way to the detector differs. On the supposition that all the photons are produced inside the primary beam and the production direction is completely isotropic the calculation of the detecting probability simplifies. Its just necessary to calculate the solid angle the photons must be produced to get detected and divide it through the 4π of the complete solid angle. Is the probability known for every distance of the production spot, it is possible to calculate a geometrical weight function or a response function of the detector.

To perform the respective integral in equation 5.2 the actual angles must be used.

$$I = \int_{\alpha_1}^{\alpha_2} \sin\left(\alpha\right) \, d\alpha \, d\phi \tag{5.2}$$

Since the photon production as well as the photon detection is completely symmetric regarding the angel ϕ the integration over ϕ gives 2π As apparent from figure 5.51 the

integration over the polar angel θ has to be performed only from α_1 to α_2. So the integration results in 5.3.

$$I = 2\pi \left(\cos(\alpha_1) - \cos(\alpha_2)\right) \tag{5.3}$$

The values of α_1 and α_2 are determinable by geometrical functions as can be seen from figure 5.51.

$$\tan\left(\alpha_1\right) = \frac{r}{x + \frac{d}{2}} \tag{5.4}$$

$$\tan\left(\alpha_2\right) = \frac{r - c}{x - \frac{d}{2}} \tag{5.5}$$

So using the equations 5.4, 5.5 and the following relation 5.6

$$\cos(\arctan(y)) = \frac{1}{\sqrt{y^2 + 1}} \tag{5.6}$$

to calculate the integral leads to the geometrical weight function 5.7 which is also shown in figure 5.52 on page 76

$$W = \frac{I}{2\pi} = \frac{1}{2} \left(\frac{1}{\sqrt{\left(\frac{r}{x+d/2}\right)^2 + 1}} - \frac{1}{\sqrt{\left(\frac{r-c}{x-d/2}\right)^2 + 1}} \right) \tag{5.7}$$

If the production function of the photons is now linked to this weight function by the mathematical operation of a convolution, the result will be the function of the detected photons outside of the target material. Figure 5.53 on page 76 contains the different functions for the produced photons, the detected photons and the convolution. The count rates of all three functions are per primary carbon ion. It become obvious that the count rates of the red coloured function of the detected photons is lower compared to the photon productions because of absorption and scatter effects. The blue line describes the calculated convolution function and as can be seen the behaviour of the function is the same as the behaviour of the function of the detected photons. The differences of the count rates are again a consequence of the absorption and scatter effects which are not considered in the used weight function. Although the investigations shown in this section used ideal collimator, there were still influences on the detected photons by the scattering and the geometry of the simulation. Nevertheless a simple calculated weight function allowed to link the different measurement methods.
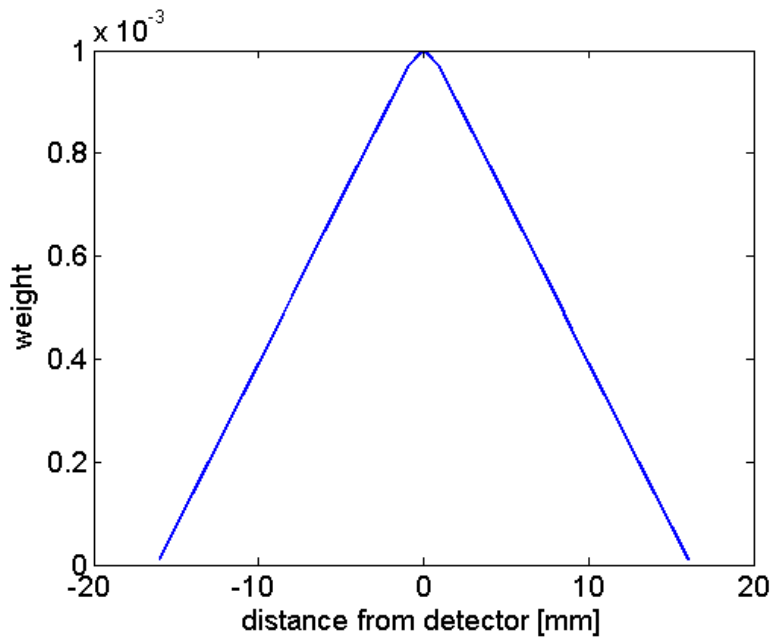
Figure 5.52: Geometrical weight function for the influence of the produced photons on a detection area according to their origins.
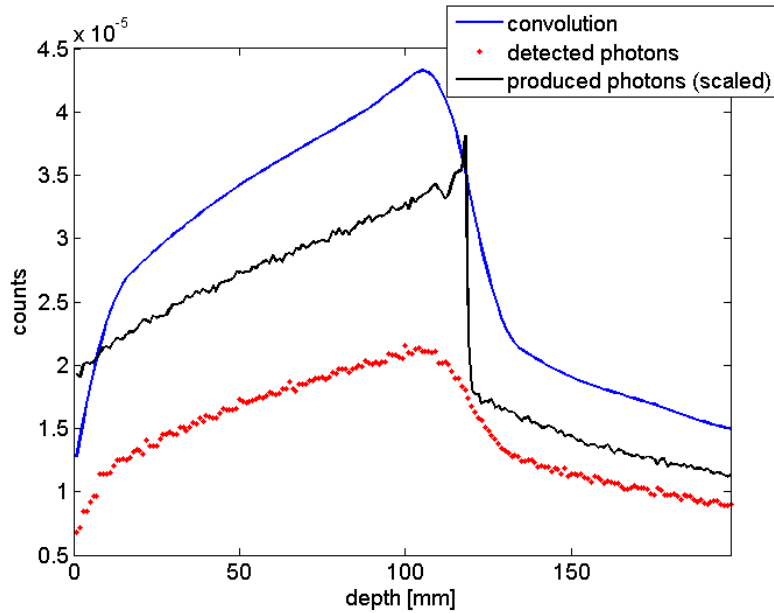
Figure 5.53: Detected photons compared to the convolution in an energy range from 2.3-6 MeV for carbon ions impinging on a water target at 240 MeV/u for a setup with ideal collimators. [3]

6 Summary and Outlook

In the course of this master thesis basic investigations on the use of prompt gamma radiation in iontherapy to monitor the dose delivery were carried out. First of all the accuracy of the used simulation tool called GATE was tested by simulating the mean free path length of photons in different materials and comparing the results with measured values provided by the Nist (National Institute of Standards and Technology) database. With a mean observational error of under one percent the standard hadrontherapy parameters for the physics processes in GATE were used for the following studies. Investigations were focused on the scattering of gamma rays and the attenuation of a photon beam in different biological materials and for different primary energies corresponding to the most prominent peaks in the energy spectrum of produced prompt γ rays. Although the shape of a photon beam, the beam attenuation and the scatter characteristics of a single photon are depending on the primary energy, the penetration depth and the irradiated material, the position of the source of the photons was always determinable. Furthermore the photon production of a carbon ion beam irradiating a water target was examined to find parameters of the produced photons which are linked to the position of the Bragg peak. Although especially the photons of the most prominent peaks of the energy spectra showed distortions it was possible to find valuable energy ranges. Most promising are the photons between 2.3 and 6 MeV since their production function shows a significant drop at the Bragg peak which is suitable to recalculate the position of the Bragg peak by measuring the prompt γ rays outside of the irradiated target. While further investigations on the shape of the beam and other parameters were made, also the relation of the photon production to the photon measurement outside the target was investigated. This was realized by a geometrical weight function, which did not include any physical processes but the geometrical setup and allowed to link the simulated measurement with the production inside the target at high accuracy.

The next steps would be to improve the sensitivity between the photon measurement outside the target and the production respectively the position of the Bragg peak inside the irradiated material. Better performance can be achieved by improving the response function by including all the important physical processes, developing an algorithm to recalculate the origins of the measured photons and an additional search for more para-

meters of the photon production with sensitivity to the Bragg peak position. Combined with an improved detector setup to avoid unwanted radiation background and influences a way to calculate the position of the Bragg peak in 3 dimensions has to be found. Furthermore the results of this and of passing thesis have to be proven by real measurements and it has to be shown that the recalculation of the Bragg peak also works under realistic conditions.

Bibliography

[1] E. Testa et al. Monitoring the Bragg peak location of 73 MeV/u carbon ions by means of prompt gamma ray measurements. *APPLIED PHYSICS LETTERS*, 93, 2008.

[2] G. Goretzki. *Medizinische Strahlenkunde: Physikalisch-technische Grundlagen.* Urban & Fischer publishing company, 2nd edition, 2004.

[3] Andreas Pichler. Simulation studies for the Bragg peak determination using prompt gamma rays in ion therapy. Master's thesis, Vienna University of Technology, 2013.

[4] D. Schardt et al. Heavy-ion tumor therapy: Physical and radiobiological benefits. *Reviews of modern physics*, 82(1):383–425, 2010.

[5] Ute Linz. *Ion Beam Therapy.* Springer-Verlag, 2012.

[6] Harald Dichtl. Monte Carlo Simulationen von prompt Gamma Emissionen bei der Strahlentherapie mit Ionen. Master's thesis, Studiengang Medizintechnik, Linz Fachhochschul-Studiengnge Obersterreich, June 2013.

[7] K. Parodi. PET Monitoring of hadrontherapy. *Nuclear Medicine Review 2012*, 15:C37–C42, 2012.

[8] S. Agostinelli et al. Geant4a simulation toolkit. *Nuclear Instruments and Methods in Physics Research, Section A*, 506:250–303, 2003.

[9] www.opengatecollaboration.org, 2013.

[10] S. Jan et al. GATE V6: a major enhancement of the GATE simulation platform enabling modelling of CT and radiotherapy. *Physics in Medicine and Biology*, 56:881–901, 2011.

[11] http://wiki.opengatecollaboration.org/index.php/Users Guide V6.2,, 2013.

[12] National Institute of Standards and Technology. http://www.nist.gov/index.html, 2003.

[13] National Institute of Standards and Technology. X-Ray Mass Attenuation Coefficients. http://physics.nist.gov/PhysRefData/XrayMassCoef/ComTab/water.html, 2013.

[14] http://www.medaustron.at,, 2013.

[15] S. Agostinelli et al. Geant4a simulation toolkit. *Nuclear Instruments and Methods in Physics Research, Section A*, 506(3):250–303, Sep 2003.